UNIVERSITÀ DEGLI STUDI
DI MILANO

Doctorate of Integrated Biomedical Research

XXXIst Cycle

Laboratory of Physiomechanics of Locomotion

Doctoral Research Thesis

The damped oscillations of passive limbs and their role in human locomotion mechanics

Alex Moorhead
R11435

Tutor: Prof. Alberto E. Minetti
Department of Pathophysiology and Transplantation

Table of Contents

Abstract

The mechanics of locomotion classically take into account the work done by muscle force to raise and accelerate the body center of mass and to accelerate limbs with respect to it at each step. This last component, named Internal Work (W_{INT}), considers only the cost to overcome segment inertia, inherently assuming frictionless joints. Thus, the unavoidable damping opposing segmental oscillation due to anatomical structures within or around the pivoting centers has never been measured so far.

The frictional coefficient (b, N·m·s·rad^{-1}) of such a biological rotational damper has been here assessed by sampling the time course of passive oscillation (with respect to the vertical axis) of upper and lower limbs and by analyzing its motion. This experiment (straight pendulum) was performed to assess joint energy dissipation during the swing phase of locomotion. A custom mathematical model, leading to a 2nd Order Non-Linear Ordinary Differential Equation, allowed to infer b values for upper (b_{UU} = 0.39 ± 0.08) and lower (b_{UL} = 2.24 ± 0.56 N·m·s·rad^{-1}) limbs in 16 healthy males. Phase planes ensured that no muscle activity was involved. In the same population, the passive swing of a lower limb, behaving as an inverted pendulum after a push (body upside-down), was also sampled while loading the leg as to replicate the compressive stress to which the hip joint is exposed during stance phase. Loads ranged from 0 N (mass of leg only) to 118 N. Damper values (b) for the inverted swing of a loaded lower limb increased with the load and ranged from 4.89 ± 1.29 to 8.92 ± 1.74 N·m·s·rad^{-1}.

The influence on locomotion mechanics has been here evaluated. In walking, for instance, each step includes 3 'passively' swinging, unloaded segments (2 upper

limbs and the swinging lower limb with joints under tensile stress) and 1 'actively' oscillating, almost fully loaded segment (stance lower limb, joint under compressive stress). The actual experimental results have been combined to provide an estimate of the internal mechanical work due to tissue and joint damping. In walking that is comparable (and should be added) to the estimate obtained by means of a kinematics-based model (Minetti, 1998) and experimental data from the literature of the traditional 'kinematic' W_{INT}. In the discussion, the potential overestimation and underestimation of those two types of internal work are presented, together with the implications of the presented additional work (and its metabolic equivalent) to the energy balance and efficiency of human locomotion.

Glossary

COM	Center of mass
BCoM	Body center of mass
KE	Kinetic energy (J)
KEi	Kinetic energy of segment i (J)
PE	Potential energy (J)
TE	Total energy (J)
W	Work (J)
W_{EXT}	External work (J)
$W_{INT,DAMP}$	Damping internal work (J)
$W_{INT,KINE}$	Kinetic internal work (J)
W_{INT}	Overall internal work (J)
W_{TOT}	Total work (J)
b	Damping coefficient ($N \cdot m \cdot s \cdot rad^{-1}$)
b_{UU}	Damping coefficient of upper limb ($N \cdot m \cdot s \cdot rad^{-1}$)
b_{UL}	Damping coefficient of lower limb ($N \cdot m \cdot s \cdot rad^{-1}$)
M	Damping moment ($N \cdot m$)
v	Velocity (m/s)
v_{BCoM}	Velocity of body center of mass (m/s)
v_i	Velocity of segment i (m/s)
m	Mass (kg)
m_i	Mass of segment i (kg)
m_{BCoM}	Mass of body center of mass (kg)
m_L	Mass of leg (kg)
θ	Angular displacement (rad)
$\dot{\theta}$	Angular velocity ($rad \cdot s^{-1}$)
$\ddot{\theta}$	Angular acceleration ($rad \cdot s^{-2}$)
ω	Angular velocity ($rad \cdot s^{-1}$)
$\propto$	Angular acceleration ($rad \cdot s^{-2}$)
Eff	Efficiency of locomotion
C	Cost of transport ($J \cdot kg \cdot m^{-1}$)
$\dot{V}0_2ss$	Steady state oxygen consumption ($ml \cdot (kg \cdot min)^{-1}$)
$\dot{V}0_2bas$	Baseline oxygen consumption ($ml \cdot (kg \cdot min)^{-1}$)
N	Newtons
R	Distance to the COM from the proximal axis of rotation(m)
R_g	Radius of gyration from the proximal axis of rotation (m)
p_0	Radius of gyration about the COM (m)
τ	Torque moment ($N \cdot m$)
T_g	Gravitational torque moment ($N \cdot m$)
T_d	Damping torque moment ($N \cdot m$)
I	Moment of inertia ($kg \cdot m^2$)
I_o	Moment of inertia about the COM ($kg \cdot m^2$)
I_p	Moment of inertia about the proximal axis of rotation ($kg \cdot m^2$)
t	Time (s)
C_{mif}	Cost of transport due to internal damping ($J \cdot kg^{-1}m^{-1}$)

Introduction

The human body is a very complex machine designed to perform an infinite number of tasks. In a very simplified manner, the body can be described as a frame (skeleton) of levers (bones), driven by actuators (muscles). But the bones do not move in a linear sense, they rotate. For any movement to proceed, they must have a point where this rotation can happen. These points of rotation are called joints and consist of two or more opposing bone surfaces separated by a fluid lubricant. Without joints, no amount of internal force could result in movement. In fact, the joint around which force is applied, determines the movement that can occur. In humans there are three main joints which exist: fibrous, cartilaginous and synovial – synovial being the only one of which allows a high range of movement. The synovial joint is aptly named for the joint space between the two connecting bones filled with synovial fluid which is intended to lubricate the joints and reduce friction between the interacting tissues. The study of synovial joints and their lubrication has been of great interest in the research of tribology, rheumatics, and prosthetics. The lubrication present in a system determines the friction it will experience. Conversely, the friction experienced will result in oscillation behavior which identifies the lubrication present. Some of the earliest published studies regarding joint lubrication and friction date back to when Jones (1934) tested an equine stifle joint using Stanton's pendular model (1923) to determine the difference in the coefficient of friction between joint surfaces lubricated with synovial fluid, saline fluid, and dry joints (without fluid). This paper distinguished the differences between two types of lubrication, fluid film (viscous) and boundary layer (coulomb) and was one of the first studies to claim that animal joints have viscous lubrification.

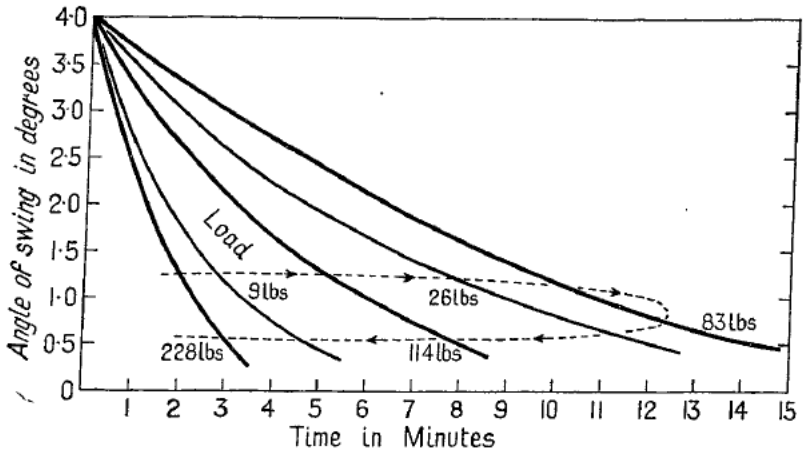

Figure 1. The oscillation behavior of an amputated human finger under loading. The curvature of the graph confirms viscous damping in the joint. (Jones, 1936)

Jones went on to support this claim in another study using an amputated human finger, effectively confirming his original findings (Figure 1). But in the years following, there were various other studies which contested this finding; claiming that coulomb friction exists in the joints. Of note, was a study by Charnley is which Jones' experiments were repeated and the findings directly disagreed with Jones' results. Charnley asserted that the damping was due to boundary interactions (Figure 2) and that attempts to reconstruct joints using viscous lubrification are doomed to failure (1960).

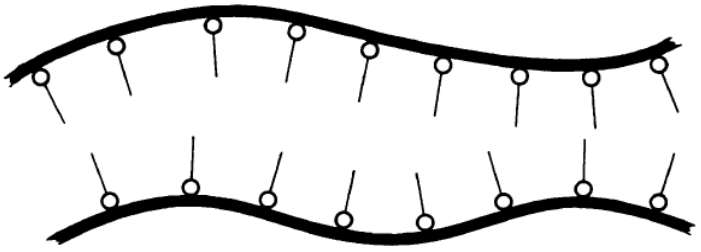

Figure 2. Graphic representation of boundary interactions which shows the surfaces to be separated by molecules with low molecular attraction between each other. (Charnley, 1960)

One primary complaint of Charnley was that Jones was making a procedural mistake by performing his tests with joints which had the ligaments still intact. This led to an investigation by Barnett and Cobbold (1962) which is highly relative to the study of *in vivo* human joints. Barnett and Cobbold tested a dog's intact limb, amputated above the knee, to measure what they considered 'friction' which really, was more likely the overall damping (1962). With all of the skin, muscle, and connective tissue still attached, they performed the first series of joint tests and observed viscous damping behavior. The skin was then removed, and the tests were repeated, followed by removing the tendons and ligaments and performing the tests one more time. Each series of tests revealed a lower coefficient of friction and once all the soft tissue was removed the damping behavior matched that of coulomb damping (surface friction) (Figure 3).

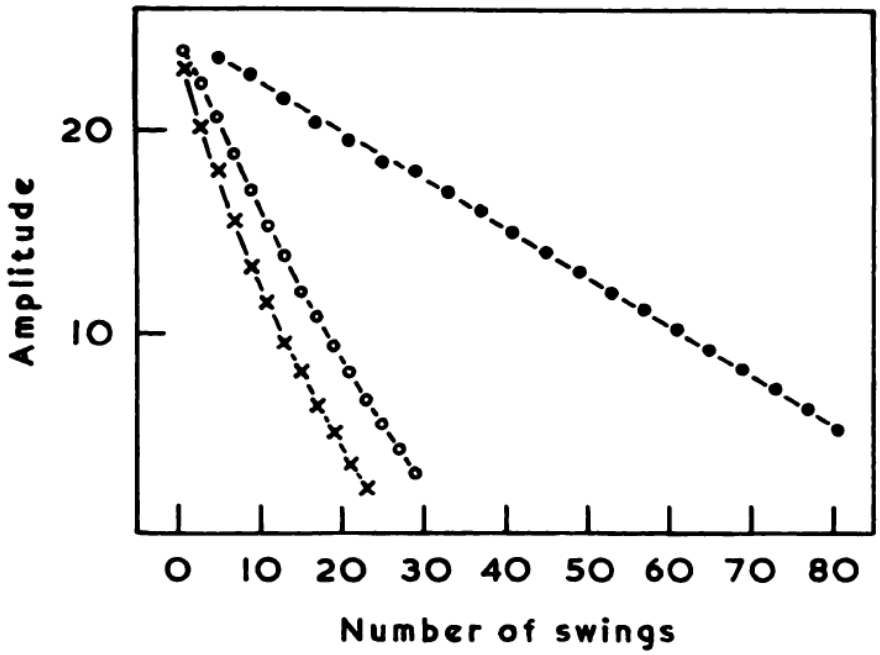

Figure 3. Plots showing the relationship between the amplitude (in arbitrary units) and the number of swings. Note the reduced damping as the skin was cut away and further reduction to a constant coefficient of friction with the tendons and ligaments removed. (Barnett and Cobbold, 1962)

✖ = Skin intact ○ = Skin excised ● = Ligaments and tendons removed

This is important because it demonstrates that even if damping is small (and coulomb) at the articular surfaces, a fully intact limb will demonstrate greater viscous damping. Often when considering the damping of joints, the primary concern is the frictional interaction between the articular surfaces. But it must be remembered that *in vivo* human joints are affected by more than just the interaction between the articular surfaces. They are surrounded by skin, muscle, tendons, ligaments, and other connective tissues. All of these tissue interactions contribute to a much larger damping effect than that measured at the articular level of excised joints. This principle was investigated and proven by Crisco et al. who showed that a mix of viscous and dry damping is the most accurate way to describe the damping nature of whole animal joints (2006). However, its direct application to the additional energetic requirements of human movement has yet be investigated.

Mechanics of human locomotion

Human, bipedal locomotion is comprised of various complex yet easily recognizable movement patterns. It allows humans to move across diverse terrains, gradients and obstacles using a wide range of chosen speeds, gaits and stride frequencies. Its utility draws attention from several fields of study. A physiologist may investigate the metabolic energy consumption of sprinting versus walking, a biomechanist can understand the mechanical work differences in walking up or down a hill, or a physiomechanist could even combine the two fields of study to understand the difference in cost of walking or running to climb a set of stairs. Whatever the chosen movement may be, it requires that the associated muscles exert force within the body perform it. One method to quantify this resulting movement is measuring the mechanical work done. Total Work (W_{TOT}, J) is the sum of the External Work done to raise (vertically) and accelerate (horizontally) the body center of mass (BCoM) within the environment (W_{EXT}, J) and the Internal Work done to accelerate the limbs with respect to BCoM (W_{INT}, J). The measurement of W_{INT} was formalized by Cavagna and Kaneko (1977) using the application of König's theorem of kinetic energy (KE) within a system to human movement. The theorem states that the total KE of a system of particles is given by the sum of the KE of a point moving with the velocity of the center of mass (v_{BCoM}), and having the mass of the whole system (m_{BCoM}), and the sum of the kinetic energy associated with each particle (KEi) moving with the velocity (v_i) relative to the center of mass having the mass (m_i):

$$\frac{1}{2}\sum_{i=1}^{n} m_i\, v_i^2 = \frac{1}{2} m_{BCoM} v_{BCoM}^2 + \frac{1}{2}\sum_{i=1}^{n} m_i\, v_i^2$$

Total energy (TE) is provided by summing the potential energy ($PE; mgh$) and the kinetic energy ($KE; \frac{1}{2}mv^2$) of the system in each plane (x, y, z).

$$TE = mgh + \frac{1}{2}\left(mv_x^2 + mv_y^2 + mv_z^2\right)$$

W_{EXT} is the sum of all increments in the PE, vertical KE and horizontal KE of the BCoM whereas W_{INT} is the sum of all the increments in the translational KE and rotational KE of the limbs in respect to BCoM:

$$W_{INT} = \sum_{i}^{n}\left(\frac{1}{2}(m_i v_i^2) + \frac{1}{2}(m_i k_i^2 \omega_i^2)\right)$$

where ω is angular velocity (rad/s) and k is the radius of gyration (m) of the limb about its center of mass (COM).

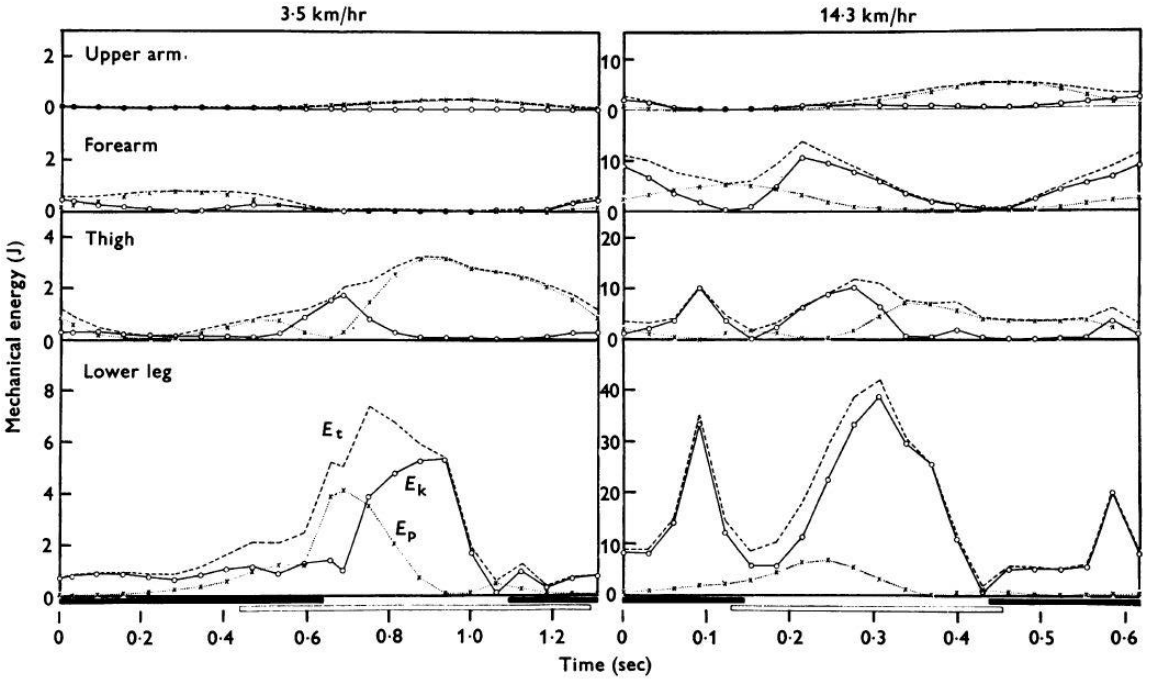

Figure 4. Graphic representation of KE (continuous line), PE (dotted line), and TE (dashed line) of different body segments during the course of two steps at the speed of walking (left) and running (right). The black bars beneath indicate stance phase (Cavagna and Kaneko, 1977).

This application of the König theorem provides the ability to divide W_{INT} and W_{EXT} and individually observe the energetic changes in each of the body segments during each phase of the gait cycle as well as the corresponding work required to do so during walking and running as shown in Figure 4.

However, this method also reveals one major downfall to bipedal locomotion. The benefit of versatility provided by legged locomotion also comes with a distinct disadvantage. The limbs must continuously oscillate about to body to maintain movement. This is common across all legged gaits. The two most commonly used human gaits are walking and running. Both walking and running share a common footfall pattern. Each stride is comprised of alternating left and right steps consisting of a swing and stance phase. From this point on, walking and running vary greatly. In walking, there will always be at least one foot in contact with the ground as well as a double contact phase when both the right and left foot are in the stance phase. In running, there will never be a time when both feet are in the stance phase and there is also an additional flight phase in which both feet leave the ground. A third less common yet important gait is skipping. In skipping there is a double contact phase as in walking, and a flight phase as in running, but the left and right footfall sequence is dependent upon the type of skipping performed: mono-lateral, in which the same foot always leads, or bi-lateral in which the leading and trailing foot alternate during each stride. The inevitable fact of legged locomotion is that as long as humans want to move, they must cyclically move their limbs. This nonstop movement of the limbs comes at a metabolic and mechanical energetic cost which makes legged locomotion relatively inefficient. Efficiency of locomotion (Eff) is evaluated as the ratio between total mechanical cost and net metabolic cost:

$$Eff = \frac{W_{TOT}}{C}$$

The measurement of C (J/(kg · m)) is not highly debated. It is evaluated as the difference between oxygen consumption during steady state exercise ($\dot{V}0_2ss$ (ml 0_2/(kg·min)) and the oxygen consumption during baseline metabolism ($\dot{V}0_2bas$ (ml 0_2/(kg·min)) divided by the velocity (v; m/s):

$$C = \frac{\dot{V}0_2ss - \dot{V}0_2bas}{v}$$

$\dot{V}0_2$ is multiplied by the energetic equivalent of the respiratory exchange ratio (RER) to calculate J of energy consumed. However, there is less confidence in the accuracy of the calculation of W_{TOT} due to the seemingly neglected or immeasurable energetic cost discrepancies in the calculation of W_{INT}. As Minetti (2011) explains, internal work includes forms of work which do not result in the 'external' kinetic part; namely, the 'viscous' internal work. Other sources of internal work include cardiac work, isometric muscle contractions and the internal damping due to tissue interactions. The current calculation of W_{INT} evaluates only the kinetic internal work and should be considered the lower limit of W_{INT} causing an under evaluation of W_{TOT}. Since determining Eff requires evaluating the interplay between W_{TOT} and C it is important that W_{TOT} is reliably and accurately measured. Doing so requires investigating how to quantify and include the additional sources of W_{INT}. As shown, the body is constantly subjected to damping due to tissue interactions within the limbs which dissipate energy during movement. An additional positive internal work must be performed to overcome these dissipative forces and maintain locomotion. At present, the existing paradigms for measuring the mechanical W_{INT} of locomotion do

not account for the present internal, viscous damping and the and the relative additional work required to maintain locomotion. This should not be neglected as it can greatly increase the amount of W_{INT} and therefore W_{TOT} which, in turn, without an equivalent increase in the cost of transport would result in a great increase in the Eff of locomotion. Pendulums have been proven in studies to be a suitable model for measuring the damping within joints. When the relationship is known between the angular and timing measurements of a pendulum, basic assumptions can be made regarding its damping properties (Unsworth et al., 1975a).

Theoretical Framework

Damped harmonic motion

Harmonic motion is present in and essential to daily life. It occurs in the turn of a piston in a car engine, the transmission of sound of instruments, and the oscillation of human limbs during locomotion. Free harmonic motion is not driven or damped. A displacement or acceleration applied to the system causes an imbalance of forces resulting in symmetric oscillation occurring about an equilibrium position. Kinematically, velocity is maximal, and acceleration is zero as oscillation passes through the equilibrium. Conversely, velocity is zero and acceleration is maximal at the furthest displacements.

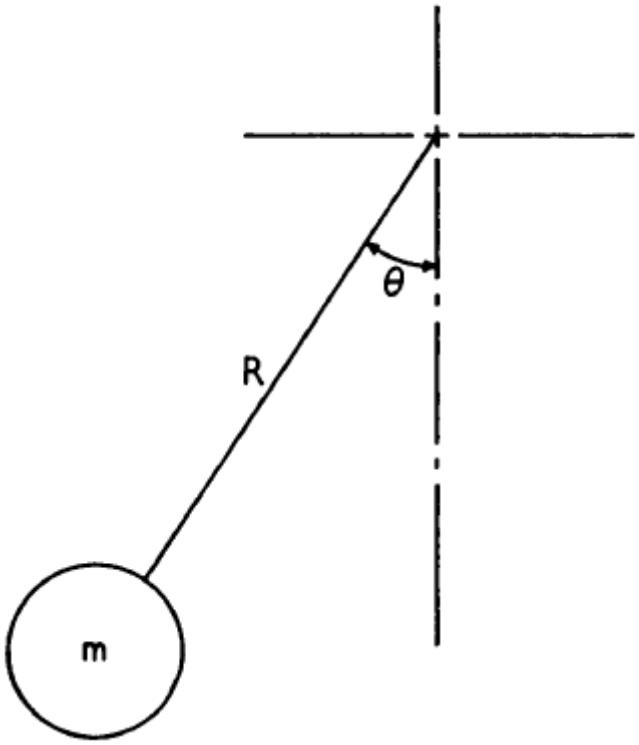

Figure 5. Diagrammatic representation of a simple pendulum. (Unsworth et al., 1975b).

This can be understood kinetically by describing the swing of a simple pendulum (Figure 5). Work (W) is done to vertically raise a mass (m) connected to a weightless wire by a specific height (h), adding potential energy ($PE = mgh$) to the system. The

m is released and accelerated by gravity (g; 9.8 m·s^{-2}), immediately beginning to transform PE into kinetic energy ($KE = \frac{1}{2}mv^2$). After reaching the bottom of the swing, the pendulum starts to rise again and KE is transformed back into PE. Modeling this pendulum with free oscillation, there is no damping force to slow the pendulum, and it would oscillate indefinitely as KE and PE are continually exchanged. In real systems, it is known that a simple pendulum does not exist since eventually all oscillations are brought to rest. The process by which oscillations are steadily diminished is known as damping and can take any of several forms, or even more than one (Steidel, 1989).

Types of damping

Viscous:

Viscous damping is the most commonly used damping mechanism and can be used to describe a shock absorber, a piston in a cylinder or a journal in a bearing. However, it is often used to describe other forms of damping when the dissipative forces are small. The damping force is opposite to the direction of velocity and is defined by variables which are lumped into a constant of proportionality (c). Since the variables which control energy dissipation are represented in the single constant c, the equation of motion is a 2nd degree linear differential equation:

$$-kx - c\dot{x} = m\ddot{x}$$

$$m\ddot{x} + c\dot{x} + kx = 0$$

Therefore, the physical the time – displacement curve will assume one of three shapes based upon the value of the under the radical of the general solutions:

$$\sqrt{\left(\frac{c^2}{4m^2}\right) - \left(\frac{k}{m}\right)}$$

Case 1. Overdamped – $\left(\frac{c^2}{4m^2}\right) > \left(\frac{k}{m}\right)$ This is the only case with real solutions. The system is so heavily damped that it cannot oscillate. It will asymptotically approach but never reach equilibrium. This can be observed in the damping of automatically closing doors.

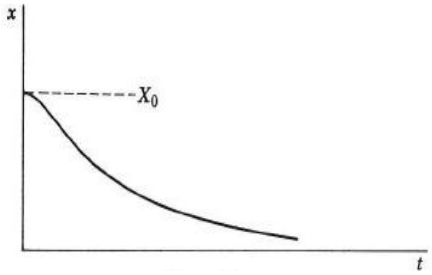

Case 2. Critically damped – $\left(\frac{c^2}{4m^2}\right) = \left(\frac{k}{m}\right)$ In this case, the terms under the radical are equal and so the solution is zero. The system still cannot oscillate but will reach equilibrium in minimal time. This is seen in the shock absorbers of cars.

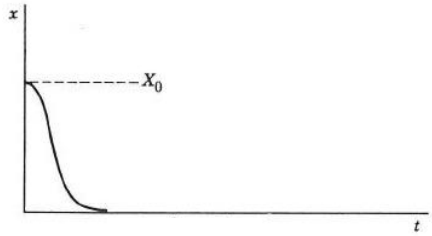

Case 3. Under Damped – $\left(\frac{c^2}{4m^2}\right) < \left(\frac{k}{m}\right)$ Damping in this case is relatively small and results in oscillation about the equilibrium. The term under the radical is negative and the roots are not real.

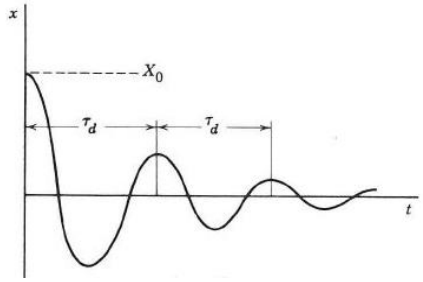

Since underdamped viscous damping allows consecutive oscillations, the energy dissipation can be defined in relation to the amplitude of each swing. In a viscously under damped oscillator, each cycle amplitude will be logarithmically related to the immediately prior oscillation amplitude:

$$X_n = X_0 e^{-\left(\frac{c}{2m}\right)\tau_d}$$

Being that the amplitude is a representation of the energy in the system, the

energetic dissipation will also have a logarithmic decrement with each oscillation.

Hysteretic:

Hysteretic damping is also known as solid or structural damping. All of which refer to the internal damping of a system under repeated elastic strain. At low frequencies this can be modeled as a viscous damper in parallel with an elastic spring. Eventually however, increased frequency will render the viscous approximation model inaccurate. In a viscous approximation the damping increases whereas hysteretic damping is opposite. The hysteretic damping of a system is due to the heat flow during the repeated bending of the material. As the frequency of that strain increases, the time for heat flow decreases and subsequently, so does the damping. The energy dissipation (ΔU) is dependent upon the amplitude of motion (X) and a frequency sensitive spring constant (h) leading to a logarithmic decrement:

$$\Delta U = \pi h X^2$$

Coulomb:

Also known as dry friction damping, Coulomb damping opposes motion independent of displacement, velocity or acceleration. It is dependent only on the normal forces of the interacting surfaces. The product of the weight (N) and the frictional coefficient (μ) between the surfaces determine the frictional force (μN). Oscillatory motion is maintained by a spring modulus (k). As such, the system will oscillate according to the ratio between the two forces ($\mu N/k$). Each successive amplitude will reduce by:

$$4\left(\frac{\mu N}{k}\right) : X_{n+1} = X_n - \left(\frac{4\mu N}{k}\right)$$

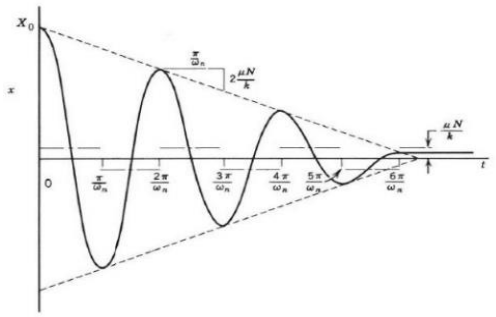

Figure 6. Linear decrement of oscillations in a system with Coulomb damping.

This results in a linear decrement between oscillations, eventually stopping motion. It should be noted that technically, coulomb damping is at least minimally present in all real systems since it is the only damping which can fully stop motion.

Cyclic Energy Dissipation

As explained, each form of damping results in a predictable decrement of energy which results in a relatively smaller maximum displacement with each passing oscillation. Plotting the successive displacements on a semilogarithmic graph in relation to each cycle as seen in Figure 7 offers a convenient way to identify the damping present in systems.

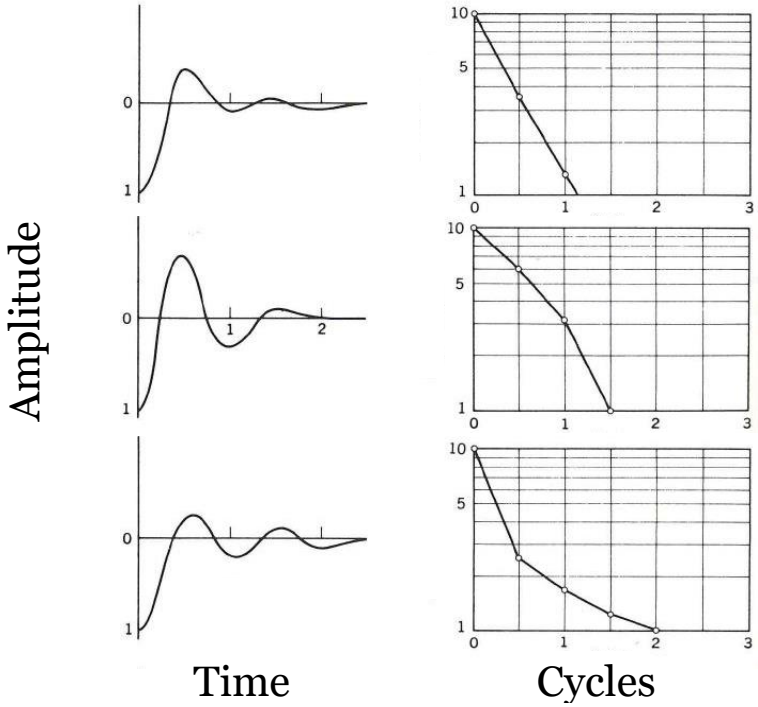

Figure 7. Time – displacement curves of oscillators under viscous (top), hysteretic (middle), and dry (bottom) forms of damping and their relative semi-logarithmic plots.

Since viscous damping follows an amplitude dependent energy dissipation, plotting

the max oscillation amplitudes on a logarithmic scale will result in a liner graph. Meanwhile, the energy dissipation of a hysteretic damper is both amplitude and frequency dependent. On a semilogarithmic plot, its oscillation amplitudes will result in a concave downward graph. Finally, dry damping energy dissipation is constant with each oscillation, so plotting its oscillation amplitudes on a semilogarithmic plot will show a concave upward graph.

Damping identification

Using these concepts, the upper and lower limbs were modeled as damped biological oscillators to identify which damping is present. Angular displacement of the distal marker was tracked on each limb in relation to its axis of rotation. The negative angles were rendered positive, and all the maximum angular displacements, were fit with a trendline to check for the cyclic energy decay (Figure 8).

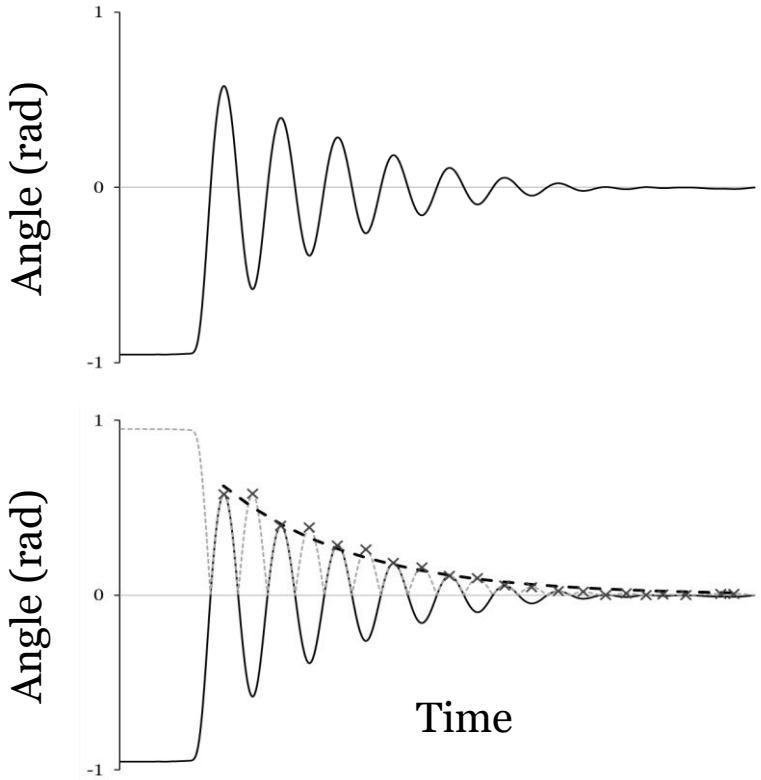

Figure 8. Example of how limb oscillations were used to identify damping. Top is the original limb oscillation. Bottom is the positively rendered values with the peaks found and a curve of best fit.

Upon initial inspection, both the upper and lower limb displayed an exponential decrement of energy with each oscillation cycle. For verification, the max oscillation displacements of all the straight tests were averaged in relation to their first oscillation and plotted against the number of oscillations. Figure 9 shows that exponential decrement was common across the cyclical max displacements of all subjects, indicating either viscous or hysteretic damping. To distinguish which damping is present, the values were plotted on a semilogarithmic plot (Figure 10).

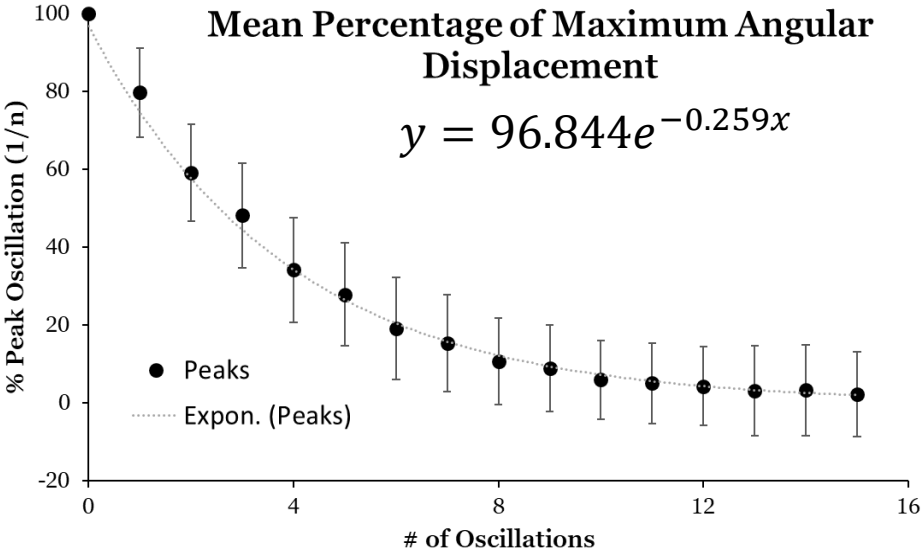

Figure 9. Mean ± SD of mean maximal oscillation displacements per swing across all straight lower limb oscillation tests.

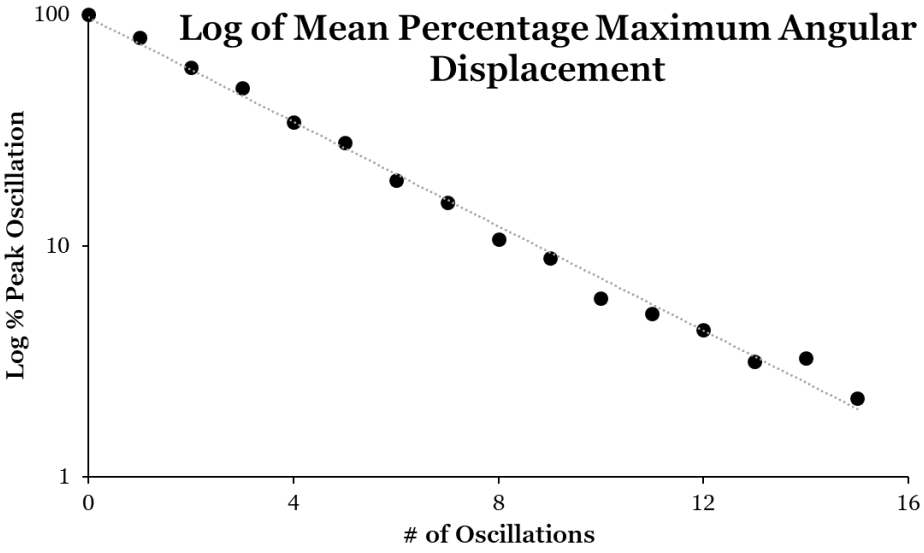

Figure 10. Mean of all maximal oscillation displacements per swing across all straight lower limb oscillation tests plotted on semilogarithmic scale.

The linear behavior of the semilogarithmic plot indicates that the energy dissipation within human limbs is due to viscous damping.

Math Model

The theory

The following deals with the dynamics of a pendulum affected by gravity and a viscous damping torque: the first part will illustrate the mathematical solution for (small) oscillations of a straight pendulum (angle θ is zero at the bottom, positive values when turning counterclockwise), the second part will consider an inverted pendulum (angle θ is zero at the top, positive values when turning clockwise). Although a single differential equation could manage both situations, a simplification introduced to solve it (see below) requires splitting the equation into two separate cases.

Damped straight pendulum

In a damped ($b;\ N \cdot m \cdot s \cdot rad^{-1}$) pendulum of mass m (and massless rod) located at a distance R from the pivoting point, because of the Moment Conservation Law:

$$I\ddot{\theta} = \sum T \tag{1}$$

where the moment of inertia, gravitational (T_g) and damping (T_d) torques are:

$$I = m\,R^2, \qquad T_g = -R\,m\,g\sin\theta \quad \text{and} \quad T_d = -b\,\dot{\theta} \tag{2}$$

When the rod also has a mass, equations (2) become:

$$I = m\,R_g^2, \qquad T_g = -R\,m\,g\sin\theta \quad \text{and} \quad T_d = -b\,\dot{\theta} \tag{3}$$

where m is the total mass of the pendulum, with the center of mass located at a

distance R from the pivot, and R_g is the radius of gyration about the pivot of the pendulum.

Thus:

$$\ddot{\theta} = -\frac{b}{m\,R_g^2}\dot{\theta} - g\,\frac{R}{R_g^2}\sin\theta \tag{4}$$

and, by assuming $\sin\theta \approx \theta$, with the restriction $-0.7 < \theta < +0.7$, corresponding to $-40^o < \theta < +40^o$ (with a mean approximation of 2.81%),

$$\ddot{\theta} = -\frac{b}{m\,R_g^2}\dot{\theta} - g\,\frac{R}{R_g^2}\;\theta \tag{5}$$

This is a 2nd Order Linear Ordinary Differential Equation (ODE) of the form:

$$\ddot{\theta} + A\dot{\theta} + B\theta\; = 0 \tag{6}$$

Where:

$$A = \frac{b}{m\,R_g^2} \quad \text{and} \quad B = g\,\frac{R}{R_g^2} \tag{7}$$

By substituting $\theta = e^{r\,t}$ into equation (6), we obtain:

$$r^2 e^{r\,t} + A\,r\,e^{r\,t} + B\,e^{r\,t}\; = 0 \tag{8}$$

or, as $e^{r\,t}$ is always > 0,

$$r^2 + A\,r + B = 0 \tag{9}$$

where solutions are:

$$r_{1,2} = \frac{-A \pm \sqrt{A^2 - 4B}}{2} \tag{10}$$

The general solution of the 2nd Order Linear ODE (eq. (6)) is:

$$\theta(t) = C_1\, e^{r_1\, t} + C_2\, e^{r_2\, t} \tag{11}$$

where $C_1$and C_2 will be set according to the initial conditions of the pendulum in terms of θ (rad) and $\dot{\theta}$ (rad/s). Depending on $A^2 - 4B = \rho$, pendulum oscillations are overdamped ($\rho > 0$) critically damped ($\rho > 0$), or underdamped ($\rho < 0$).

Our joint friction experiment is expected to provide underdamped oscillations, as suggested when observing the upper or lower limb passively behaving as a straight pendulum.

Thus:

$$r_{1,2} = \frac{-A \pm i\sqrt{4B - A^2}}{2} \tag{12}$$

and

$$\theta(t) = C_1\, e^{\frac{-A + i\sqrt{4B - A^2}}{2}\, t} + C_2\, e^{\frac{-A - i\sqrt{4B - A^2}}{2}\, t}$$

$$\theta(t) = e^{-\frac{A}{2}t}\left(C_1\, e^{i\frac{\sqrt{4B - A^2}}{2}\, t} + C_2\, e^{-i\frac{\sqrt{4B - A^2}}{2}\, t}\right) \tag{13}$$

But, due to Euler's Identity, $e^{i\,\omega\, t} = cos(\omega\, t) + i\, sin(\omega\, t)$, and

$e^{-i\,\omega\, t} = cos(\omega\, t) - i\, sin(\omega\, t)$, and with $\omega = \frac{\sqrt{4B - A^2}}{2}$;

$$\theta(t) = e^{-\frac{A}{2}t}\left(C_1\left(cos(\omega\, t) + i\, sin(\omega\, t)\right) + C_2\left(cos(\omega\, t) - i\, sin(\omega\, t)\right)\right) \tag{14}$$

Then:

$$\theta(t) = e^{-\frac{A}{2}t}\big((C_1 + C_2)cos(\omega\, t) + i(C_1 - C_2)sin(\omega\, t)\big) \tag{15}$$

or, by assimilating $C_1 + C_2$ and $i(C_1 - C_2)$ to the general constant K_1 and K_2, respectively:

$$\theta(t) = e^{-\frac{A}{2}t}\big(K_1\, cos(\omega\, t) + K_2\, sin(\omega\, t)\big) \tag{16}$$

from which, by imposing initial conditions in terms of angle and angular speed, Cauchy Problem can be solved as:

$$\theta(0) = K_1 = \theta_0 \tag{17}$$

and

$$\dot{\theta}(t) = -\frac{A}{2}e^{-\frac{A}{2}t}\big(K_1\, cos(\omega\, t) + K_2\, sin(\omega\, t)\big) + e^{-\frac{A}{2}t}\big(\omega\, K_2\, cos(\omega\, t) - \omega\, K_1\, sin(\omega\, t)\big)$$

$$\dot{\theta}(0) = \omega\, K_2 - \frac{A\, K_1}{2} = \dot{\theta}_0$$

$$K_2 = \frac{2\,\dot{\theta}_0 + A\,\theta_0}{2\omega} \tag{18}$$

Pendulum angle time course, $\theta(t)$ (eq. (16)), corresponds to

$$\theta(t) = K\, e^{-\frac{A}{2}t}\, sin(\omega\, t + \phi) \tag{19}$$

where

$$K = \sqrt{K_1^2 + K_2^2} \quad \text{and} \quad \phi = \pi\, sgn(sgn(K_2) - 1) + arctan\frac{K_1}{K_2}$$

or

$$K = sgn\,(K_2)\sqrt{K_1^2 + K_2^2} \quad \text{and} \quad \phi = arctan\frac{K_1}{K_2} \tag{21}$$

Equation (19), in extended form, is

$$\theta(t) = 2\,R_g \sqrt{m\frac{g\,R\,m\,\theta_0^2 + R_g^2\,m\,\dot{\theta}_0^2 + \theta_0\,\dot{\theta}_0\,b}{4\,g\,R\,m^2R_g^2 - b^2}}\; e^{-\frac{b}{2\,m\,R_g^2}t}\; sin\left(\frac{\sqrt{4\,g\,R\,m^2R_g^2 - b^2}}{2\,m\,R_g^2}\,t + \right.$$

$$\left.\pi\, sgn\left[sgn\left(\frac{2\,R_g^2\,m\,\dot{\theta}_0 + \theta_0\,b}{\sqrt{4\,g\,R\,m^2R_g^2 - b^2}}\right) - 1\right] + arctan\left(\theta_0\frac{\sqrt{4\,g\,R\,m^2R_g^2 - b^2}}{2\,R_g^2\,m\,\dot{\theta}_0 + \theta_0\,b}\right)\right) \tag{22}$$

or

$$\theta(t) = 2\,R_g\; sgn\left(\frac{2\,R_g^2\,m\,\dot{\theta}_0 + \theta_0\,b}{\sqrt{4\,g\,R\,m^2R_g^2 - b^2}}\right)\sqrt{m\frac{g\,R\,m\,\theta_0^2 + R_g^2\,m\,\dot{\theta}_0^2 + \theta_0\,\dot{\theta}_0\,b}{4\,g\,R\,m^2R_g^2 - b^2}}$$

$$e^{-\frac{b}{2\,m\,R_g^2}t}\; sin\left(\frac{\sqrt{4\,g\,R\,m^2R_g^2 - b^2}}{2\,m\,R_g^2}\,t + arctan\,\theta_0\frac{\sqrt{4\,g\,R\,m^2R_g^2 - b^2}}{2\,R_g^2\,m\,\dot{\theta}_0 + \theta_0\,b}\right) \tag{23}$$

In these solution equations, the damping factor b is the only unknown variable as all the other symbols, except from the ones related to initial conditions (θ_0 , $\dot{\theta}_0$), are set by the anatomical characteristics of each subject and the inertial property of the limb (+load for the inverted pendulum).

From the comparison between the experimental and predicted time courses of lower limb oscillations, iteratively obtained for a wide range of b values, the best estimation

of damping could be obtained for each experimental condition. An alternative, of similar complexity, is a non-linear custom regression (eq. 22), fed with the data of the time course of pendulum oscillation, where the damping coefficient b could be estimated.

The easiest procedure is to extract from experimental oscillations the pendulum angles (and timing) at the successive swing inversions, rectify them and performing an exponential regression (the true one (e.g. LabView, National Instruments, US or Grapher, Apple Computers, US), not the linearized version (Excel, Microsoft, US), see below), in the form:

$$y = p\, e^{qt} \tag{24}$$

which would estimate the term q ($= -\frac{A}{2}$ of eq. (22)) from which b can be obtained as

$$b = -2\, m\, R_g^2\, q\ . \tag{25}$$

Damped inverted pendulum

The above solution for the straight pendulum cannot be used for the inverted pendulum because the assumption $\sin\theta \approx \theta$ does not hold for angles with operative range around π. To use the same simplification, reference angle for zero should be in the middle of its new operative range, i.e. when the pendulum is at the top of its trajectory. We also introduced positive angles when moving clockwise.

Equations (2) and (3) should be changed into:

$$I = m\, R^2,\ T_g = R\, m\, g \sin\theta \quad \text{and} \quad T_d = -b\, \dot{\theta} \tag{26}$$

and

$$I = m\,R_g^2\ ,\ T_g = R\,m\,g\sin\theta \quad \text{and} \quad T_d = -b\,\dot{\theta} \tag{27}$$

The successive equations for the straight pendulum still hold, up to eq. (11) if:

$$A = \frac{b}{m\,R_g^2} \quad \text{and} \quad B = -g\frac{R}{R_g^2} \tag{28}$$

Now $\rho = A^2 - 4B$ is always positive and although improper for describing the travel of a damped inverted pendulum from side to side while passing through the top point, the dynamics gets closer to an overdamped condition, which is associated to a different, much simpler solution.

In this case the solution of the 2nd Order Linear ODE (eq. (6) and (10)) is:

$$\theta(t) = C_1\,e^{M\,t} + C_2\,e^{N\,t} \tag{29}$$

where

$$M = \frac{-A+\sqrt{A^2-4B}}{2} \quad \text{and} \quad N = \frac{-A-\sqrt{A^2-4B}}{2} \tag{30}$$

From differentiation of equation (30), angular speed can be obtained as:

$$\dot{\theta}(t) = C_1\,M\,e^{M\,t} + C_2\,N\,e^{N\,t} \tag{31}$$

Equations (29) and (31) allow to estimate the value of $C_1$and C_2according to the initial conditions, $\theta_0 = \theta(0)$ and $\dot{\theta}_0 = \dot{\theta}(0)$:

$$C_1 = \frac{\dot{\theta}_0 - N\theta_0}{M-N} \quad \text{and} \quad C_2 = -\frac{\dot{\theta}_0 - M\theta_0}{M-N} \tag{32}$$

leading to the closed form of equations (29) and (31):

$$\theta(t) = \frac{(\dot{\theta}_0 - N\theta_0)\, e^{M\,t} - (\dot{\theta}_0 - M\theta_0)\, e^{N\,t}}{M-N} \tag{33}$$

$$\dot{\theta}(t) = \frac{(\dot{\theta}_0 - N\theta_0)\, M\, e^{M\,t} - (\dot{\theta}_0 - M\theta_0)\, N\, e^{N\,t}}{M-N} \tag{34}$$

Differently from the straight pendulum experiments, only one inverted swing is obtained at a time, from which the damping factor b could be estimated. Similarly, rather, a non-linear, custom regression could be used to estimate M and N, thus A, and consequently, b. Also, in this case, this process looked cumbersome and complex, so a different analysis strategy was developed.

Known data from the single experimental swing, within an angular range where the dynamics is unaffected by the pushing and stopping of the pendulum, are the initial and final angle (θ_0 and θ_{end}, with respect to the vertical), the initial and final angular speed ($\dot{\theta}_0$ and $\dot{\theta}_{end}$), and the time duration of the oscillation from the initial angle to the final one (t_{swing}). A software routine has been designed (LabView, National Instruments, US), to generate a multitude of angle time courses (equation (33)) with a resolution of 0.1 ms, starting from the same initial conditions (θ_0 and $\dot{\theta}_0$), each of them depending on a given b value chosen from a realistic and highly resoluted (step 0.001 N m s/ rad) wide range. The algorithm selected b values associated to time courses capable to reach both θ_{end} and $\dot{\theta}_{end}$ after a time t_{swing}. Thresholds for the allowed approximation of the three simultaneous goals where manually chosen as to obtain a coefficient of variation of b ($CV_b = \frac{SD_b}{\bar{b}}$) smaller than 1%.

Another method is to check at which b value the oscillation reaches the minimum angular speed at the same interval from the end of the push as during experiments. By differentiating equation (34) and equating the result to zero, the timing of the minimum angular speed ($t_{\dot{\theta}_{MIN}}$) can be obtained as:

$$t_{\dot{\theta}_{MIN}} = ln\left(\sqrt[M-N]{\frac{(\dot{\theta}_0 - M\theta_0)N^2}{(\dot{\theta}_0 - N\theta_0)\,M^2}}\right) \tag{35}$$

or

$$t_{\dot{\theta}_{MIN}} = \frac{ln\left(\frac{\dot{\theta}_0 - M\theta_0}{\dot{\theta}_0 - N\theta_0}\right) + 2(ln\,N - ln\,M)}{M-N} \tag{36}$$

Similar thresholds were allowed to detect the reach of a close approximation with experimental $t_{\dot{\theta}_{MIN}}$.

Statistical procedure

The accuracy and robustness of the illustrated data analyses, for straight and inverse pendula, have been checked by generating 'reference' angle time courses where inertial properties, initial values for the dynamics, and the damping factor b were imposed (Working Model, Knowledge Revolution, US). Then those data were fed into the two processing schemes to verify b estimate accuracy and precision.

Exponential regression for analyzing the oscillation peak angles in the straight pendulum experiments deserves some extra comments. Different software packages provide exponential regression analysis according to different optimization criteria, resulting in different estimates for the same data file processed. Although the general fitting algorithm is based on Least Squares Method (LSM), the packages differ on which distance is minimized. Microsoft Excel, by applying 'Add Trendline...' after

having selected a data series in a graph (and choosing Exponential in the setting window), minimizes the sum of squared distances between the logarithm and the vertical coordinate of experimental points from the fitting line (which corresponds to the exponential curve in linear terms). In this way, the zone in the dataset where very small values (but that would happen also with very high values) appear will have a great 'weight' in generating the final exponential fitting, i.e. a remarkable discrepancy between the dataset and the regression curve could be apparent. Other software packages, as LabView (National Instruments, US, via a provided 'vi' (virtual instrument)) and Grapher (Apple Computers Inc., US, via the possibility to write a custom equation), apply LSM by minimizing the linear distance between experimental data and the 'final' regression exponential. This procedure 'equalizes' the importance of distances along the entire data set range.

The same data from simulated straight pendulum were fit with the two LSM and it was found that the sum of residuals was 97% less by using the 'linear' method than with the 'linearized (via logarithmic transformation)' one. Also, the 'nonlinearized' method (Grapher, LabView) provided exponential curves much better interpolating the experimental data along the whole operative range, and it was adopted to analyze all straight pendulum measurements.

Phase planes, i.e. graphs showing the straight pendulum oscillation in terms of angular speed vs. angle, were used to exclude trials where muscle activity was involved. In a passive, damped pendulum, phase planes show a spiral trajectory leading towards zero angle (with respect to the vertical) and zero angular speed. Any apparent deviation from the spiral was considered as produced by an involuntary muscle contraction.

The inverted pendulum analyses (Method 1: eq. (33) and (34); Method 2: eq. (35)) revealed to be more critical. Even processing simulated data provided reliable predictions of b only when initial, final conditions and their timing were very accurately measured. Particularly, the timing had to include the half time step caused by angle differentiation (to obtain angular speed), and initial angle had to be the average of the first two data points. When these precautions were adopted, the b estimates fell within 2% of the imposed value for the inverted pendulum simulation, with a Coefficient of Variation (CV) of less than 1%.

The cost to overcome the damping of the limbs during a locomotory cycle

The mechanical energy necessary to maintain a periodic oscillatory movement

$$\theta = A \sin(\omega\, t) \tag{37}$$

where A is half the angle range and ω is the frequency coefficient ($\omega = 2\,\pi\, f$, with f in Hz), of a damped pendulum with viscous friction (damping) b ($J \cdot m \cdot s \cdot rad^{-1}$), is calculated by integrating over one cycle the work rate ($\dot{W}$, W) equation of energy dissipation.

Actually,

$$\dot{W} = M\, \dot{\theta} \tag{38}$$

where the damping moment ($M, N \cdot m$) is:

$$M = b\, \dot{\theta} \tag{39}$$

and angular speed, from differentiation of eq. 37, is:

$$\dot{\theta} = A\, \omega \cos(\omega\, t) \tag{40}$$

Then, the energy dissipated by the damping effect over one cycle (W_{1c}, J) is:

$$W_{1c} = \int_0^{\frac{2\pi}{\omega}} \dot{W}\, dt = b\, A^2\omega^2\, cos^2(\omega\, t)dt \tag{41}$$

or

$$W_{1c} = \frac{1}{\omega}\int_0^{2\pi} b\, A^2\omega^2\, cos^2(\omega\, t)d(\omega\, t) = \pi\, b\, A^2\omega \tag{42}$$

In order to obtain an estimate of the mechanical cost of transport just due to the internal friction of a damped limb (C_{mif}, J· m-1), we need to calculate the distance travelled (d_{1c}, m) by a body with limbs behaving as described in eq. 37. By assuming, as in eq. 5, $\sin\theta \approx \theta$, ($-0.7 < \theta < +0.7$ rad, or $-40^o < \theta < +40^o$), and a limb length R_L(m):

$$d_{1c} = 4\, R_L \sin(A) \approx 4\, R_L\, A \tag{43}$$

Average speed $\bar{v}$ can be expressed as the distance travelled by limb extremity during half of a cycle, divided by half the oscillation period:

$$\bar{v} = \frac{2\, R_L\, A}{\frac{1}{(2\, f)}} = 4\, R_L\, fA \tag{44}$$

Thus, by combining eq. 42, 43 and 44, substituting ω and by including body mass (m, kg):

$$C_{\mathrm{mif}} = \frac{\pi^2\, b}{8\, {R_L}^2}\bar{v} \tag{45}$$

The estimate above refers to a single limb, and the mass-specific mechanical cost of transport (C_{mif}, J·kg-1·m-1), to overcome friction (damping) of all the 4 limbs in the body is:

$$C_{\text{mif}} = \frac{\pi^2 B}{8 m {R_L}^2} \bar{v} \quad (46)$$

with $B = \sum_1^4 b_i$, where bi are the damping coefficients of each proximal joint. Eq. 46 assumes the 4 limbs of the same length (R_L) and spanning the same angle range ($2A$) during locomotion.

Actually, to consider all the relevant energy dissipation of locomotion, the summation building up the variable B should include ankles.

Schematically, these are the coefficient to be included:

b1 = UPPER right limb, from unloaded swinging experiments, full cycle

b2 = UPPER left limb, from unloaded swinging experiments, full cycle

b3,1 = LOWER right limb, from unloaded swinging experiments, half cycle

b3,2 = LOWER right limb, from loaded inverted swinging experiments, half cycle

b4,1 = LOWER left limb, from unloaded swinging experiments, half cycle

b4,2 = LOWER left limb, from loaded inverted swinging experiments, half cycle

These coefficients can be reduced to 4 by considering that:

a) b1 = b2, thus bU=2 UPPER limb, unloaded swinging experiments, full cycle

b) b3,1 = b4,1, thus bL,U = LOWER limb, unloaded swinging experiments, full cycle

c) b3,2 = b4,2, thus bL,L = LOWER limb, loaded inv. swinging experiments, full cycle

Applying the developed math model required calculating the values of its defined constants; mass (m), radius to the center of mass (R), radius of gyration (R_g), initial (θ_0) and final angle (θ_{end}), and initial ($\dot{\theta}_0$) and final angular velocity ($\dot{\theta}_{end}$).

Radius to the center of mass

The m and R of both the upper and lower straight, unloaded limbs were calculated using previously anthropometric parameters previously established by Dempster (Winter, 2009). Limb length was measured as the two-dimensional (2D) distance between the markers placed at the proximal and distal joint centers (elbow and knee markers were used only to ensure that there was no angular deviation). The product of that length and the defined ratio provides R. Similarly, the limb mass (m_L) is the product of the subject's body mass and the appropriate limb ratio. Together, m_L and the limb COM coordinates ($x_L,\ z_L$) provide the weighted coordinates of the limb in each plane (mx_L, mz_L) which is necessary to calculate the R of a loaded limb. In the case of a loaded limb, the 2D coordinates of each added load ($x_i,\ z_i$) multiplied by its mass (m_i) provide the load's weighted coordinates in each plane (mx_i, mz_i). The sum of the limb's weighted coordinates and weighted coordinates of all the additional loads divided by the total mass of the system ($M;\ m_L + m_i \ldots + m_n$), gives the 2D coordinates of the of the COM:

$$x_{COM} = \frac{m_L x_L + m_i x_i \ldots m_n x_n}{M}$$

$$z_{COM} = \frac{m_L z_L + m_i z_i \ldots m_n z_n}{M}$$

R will then be the 2D distance between the axis of rotation and COM. While R remains constant in a rigid system, the location of COM will change as the limb

oscillates. Using this method to calculate the 2D COM coordinates conveniently allows the angular position (θ_{COM}) and angular velocity of COM ($\dot{\theta}_{COM}$) to be tracked across each interval of time. Since it is now known how to calculate m, R, θ_0, θ_{end}, $\dot{\theta}_0$, and $\dot{\theta}_{end}$, the final input needed is R_g. Conveniently, the R_g of unloaded limbs has already been determined from their COM, proximal end, and distal end. However, if the limb is loaded (as in the loaded lower limb tests) or if the axis of rotation happens about an abnormal location calculating the R_g requires additional computation.

Radius of gyration

In rotational movements, a torque applied to an object (τ; N·m) will result in a change to that object's angular velocity ($\propto$; rad/s^2) which is inversely proportional to the object's rotational inertia (I; kg·m^2). This is defined in the rotational equivalent of Newton's second law:

$$\tau = I \propto$$

Therefore, as implied by its unit, an object's rotational inertia is a productive of its mass and distance from the axis or rotation:

$$I = mr^2$$

This explanation of inertia expressed an object's mass as being concentrated at single point. However, a human limb is composed of various tissues with its mass distributed about its volume. Considering this, a limb's total mass (M) can be more easily expressed as the sum of the multiple segmental masses (m_n):

$$M = \sum_{i=1}^{n} m_i$$

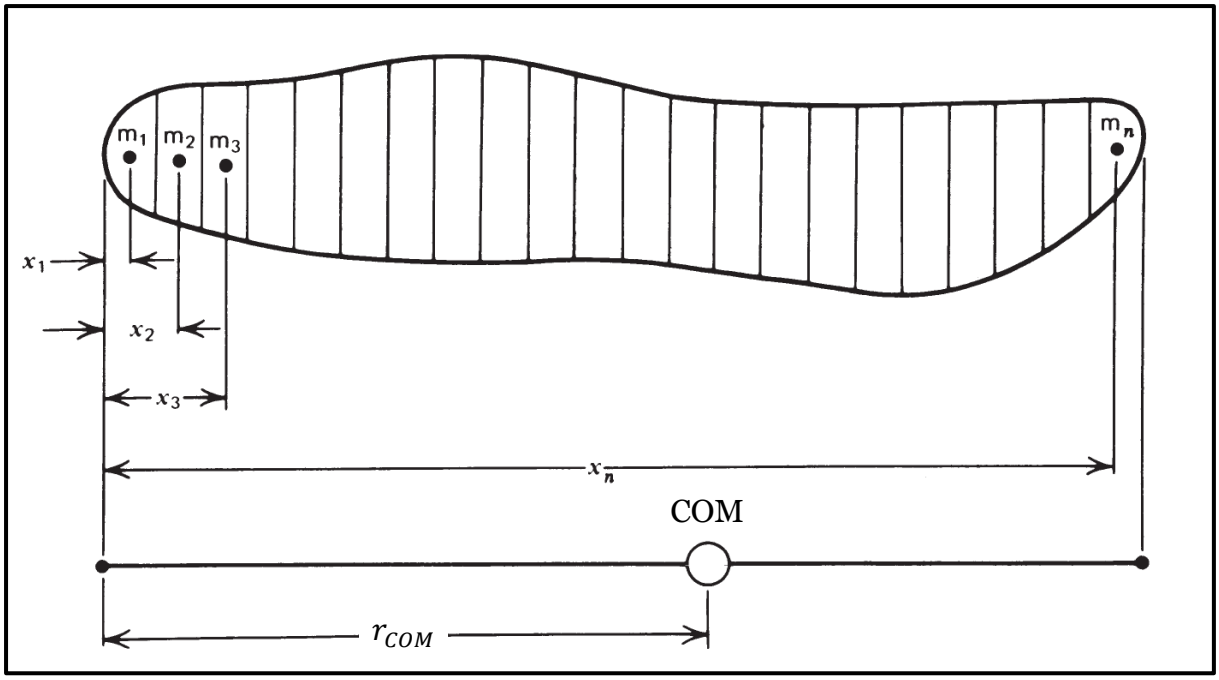

Figure 11. Location of the COM of an object relative to the segmented mass (WINTER, 2009).

Consider Figure 11. In this case, if assuming rotation from the left of the limb, each portion of the limb's mass will provide its own moment of inertia equivalent to the product of its mass (m_n) and its distance (x_n) squared (I_n=$m_n x_n^2$). The overall moment of inertia of the limb shown in Figure 11 would then be the sum of the moments of inertia of all the segments:

$$I = \sum_{i=1}^{n} m_i \, x_i^2$$

I decreases as the axis of rotation approaches the COM and will be minimal when rotation happens about the COM. Here, a theoretical division of the limb's mass into two point masses (Figure 12), will determine a distance at which these partial masses create a moment of inertia equivalent to that of the original limb moment of inertia about the COM (I_o). This distance is known as the radius of gyration (R_g, p_0):

$$I_0 = mp_0^2$$

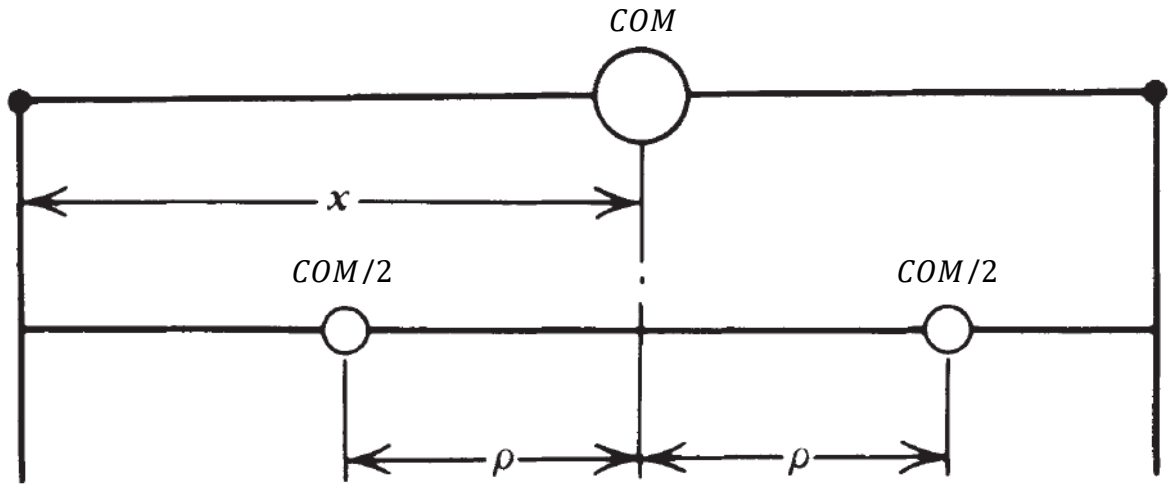

Figure 12. The radius of gyration relative to the COM. (WINTER 2009).

Since rotation of human limbs takes place about their joints rather than their COMs, in vivo measurements of inertia must also be taken about the joints. To do so requires knowing the relationship between the moment of inertia of a limb about its COM and moment of inertia of a limb about the joint center. This is possible with the parallel-axis theorem:

$$I = I_0 + mx^2$$

In fact, using this theorem, I can be determined about any point at any distance along the same axis as I_0 was calculated. Or, conversely, if I and mx^2 is known about that point, then I_0 can be determined. This was particularly applicable in finding the R_g in the loaded lower limb and ankle experiments.

Inverted lower limb

The R_g of the loaded lower limb was computed by first summing the inertia of the leg ($I_{p,L}$) and all additional masses ($I_{p,n}$) about the hip joint to give the total inertia of the system ($I_{p,SYS}$):

$$I_{p,SYS} = I_{p,L} + \sum_{i=1}^{n} I_{p,i}$$

Calculating I_p of each added load required the parallel-axis theorem. Each load's m was known and the distance was measured using the marker at its COM, meaning the last step was to calculate its I_0. This was done using references of I_0 for uniform objects. Each plate mass has a I_0 of,

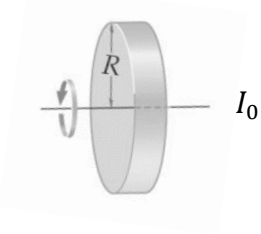

$$I_0 = \frac{1}{2mr^2}$$

So,

$$I_{p,i} = \frac{1}{2mr^2} + mx^2$$

Once $I_{p,SYS}$ has been calculated about the hip, the R_g about the hip can be found using the relationship of r, I and m:

$$R_g = \sqrt{\frac{I_{p,SYS}}{m_{SYS}}}$$

Phase planes

It was imperative to ensure that the limb oscillations were not impacted by muscular activation of the subject. This would alter the angular trajectory and later introduce error into the calculated damping value. Typically, monitoring muscle activation is done using electromyography (EMG). However, the brace and added masses limited space and therefor did not allow for proper placement of EMG sensors. Fortunately, plotting the angle against the angular velocity in a phase plane served as a useful alternative (Figure 13). Similar to a pendulum, when a limb is released to oscillate in the straight condition, it will reach a maximum velocity, decelerate, reach an angular maximum, stop, and begin swinging backwards. In a damped oscillator, the max

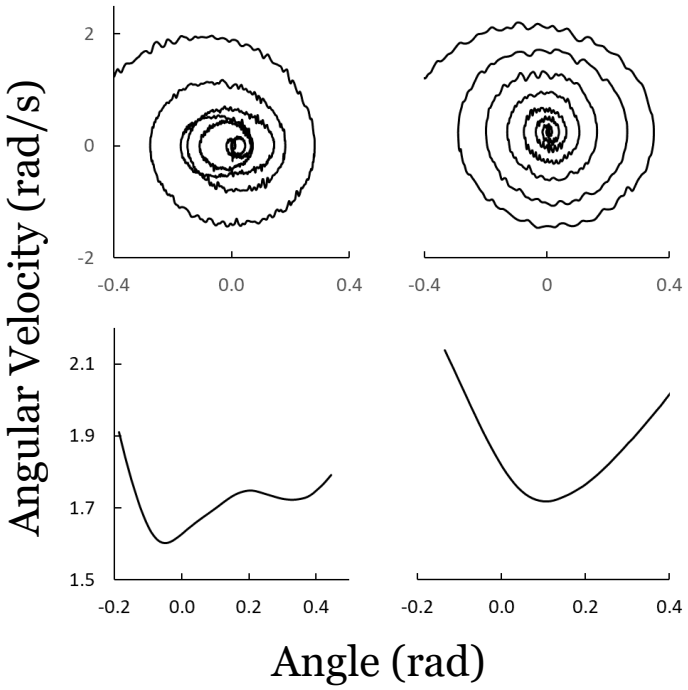

Figure 13. Examples of phase diagrams in the straight condition (top two graphs) and inverted condition (bottom two graphs) with muscular intervention (left two graphs) and free oscillation (right two graphs).

angle and velocity will decrease slightly with each oscillation. Because of this, the phase plane should show a spiral which approaches zero velocity and zero angle. Due to friction (damping) in the limbs, their phase planes should do the same unless the subject influences the swing.

In the case of the inverted limb, phase planes serve the same purpose, but must be considered in reference to a different part of the oscillation. Since the inverted experiments do not allow for recurring oscillations, only a small portion of the phase plane can be compared. This portion of the phase plane occurs just prior to and after the point where the limb is directly perpendicular to the horizontal. In this case, the limb will have already been released by the operator and gravity will be decelerating its angular velocity until the COM is directly above the axis of rotation, the hip. After

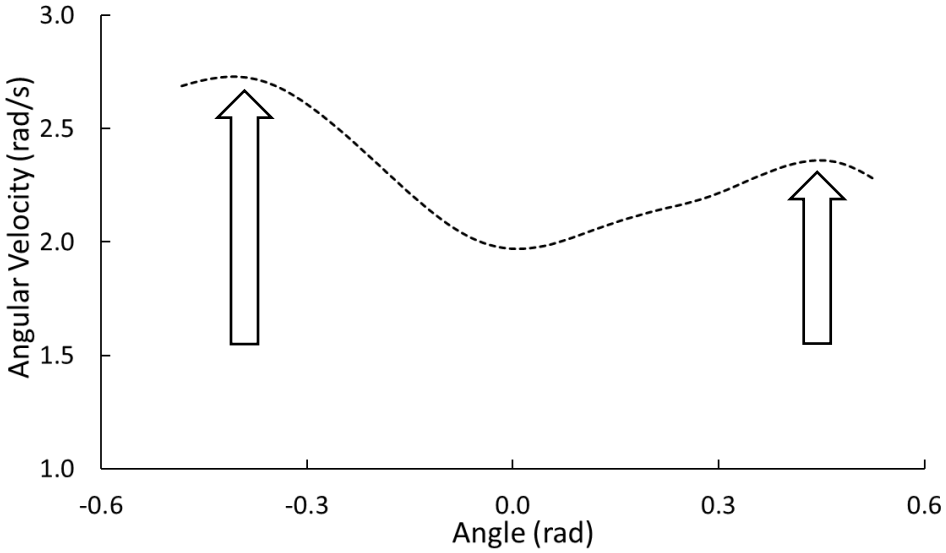

Figure 14. Untrimmed phase diagram of inverted limb swing. Left arrow showing where the push was released and right arrow where leg contacts padding.

this point, gravity begins acting as an accelerative force on the oscillation of the limb. This means the phase plane should resemble a curve with and upward inflexion approximately centered about the zero angle. If the subject activates any muscles during the swing, it will either augment or diminish the velocity of the system, causing the limb to deviate from the expected trajectory. These patterns can be visually inspected after the experiments and allow for trials to be kept or discarded. Using a similar logic, phase planes also permitted the tests to be appropriately trimmed to define θ_0, θ_{end}, $\dot{\theta}_0$ and $\dot{\theta}_{end}$. Since the leg was initially accelerated by the operator and then stopped by padding, both of these events left a signature in the

phase planes which indicated when to cut the data. As the operator released the leg, there was no longer an external acceleration and so the slope of the graph quickly changed negative. Conversely, on the opposite side, the slope would be positive as gravity accelerates the limb, until it contacts the padding at which point the slope would become negative (Figure 14).

Study Development

The established math model for this study is very sensitive to even minute differences. Using it to calculate reliable results required that the data sampled was both highly accurate and precise. To ensure that the experiments provided valuable data required the consideration of three principle constraints.

Limb stabilization

The chosen limb restraint also needed to meet three primary objectives: block movement of the non-studied joint, be customizable for each subject, and accomplish the previous tasks without occluding the reflective markers from sight of the infrared cameras. Since the upper limb is never under load during locomotion, it did not require loaded testing and mono-lateral bracing sufficed for blocking the elbow joint movement. A ridged rod was placed across the inside of the elbow joint and fixed to the arm in three places with medical tape (Figure 15). The removable medical tape made placement of the rod easily customizable to each subject without marker occlusion. The lower limb however, changes between compressive and tensile loads during locomotion which requires straight and inverted testing conditions as well as extensive bracing to restrict movement of the knee joint. Early tests used a plaster cast to brace the knee. The cast required a doctor to properly fit the cast which then had to cure and could not be altered afterward. This made it time intensive,

expensive and unable to be customized, although cutting and refitting a single cast was attempted (Figure 16). Size differences between subjects made the cast ineffective at blocking joint movement on the successive subjects and cutting the cast destroyed its structural integrity which was crucial for the inverted tests. Additionally, enclosing the knee required placing its marker directly on the cast which lead to discrepancies between the knee and ankle oscillation. Inspection of the kinematic data showed that the knee marker seemed to oscillate smoothly while the ankle marker displayed perturbations in its oscillation, revealing knee movement within the cast. This led to opting for an adjustable brace which allowed for better bracing and marker placement directly on the skin. The second proposed brace was adjustable and allowed for the desired marker placement (Figure 17) but was also much smaller and allowed for too much flexion at the knee joint. Finally, a leg brace was chosen which extended the full length of the leg and had metal bracing along the medial and later sides (Figure 17). This brace was ideal because it could be fit for each subject, allowed observation of all markers and blocked movement of the knee joint during both straight and inverted leg oscillations. As an added benefit, this brace offered a unique solution to attaching additional loads to the lower limb.

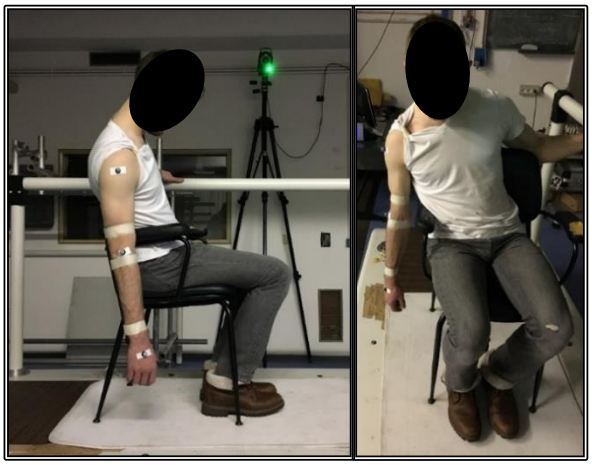

Figure 15. Seated subject with bracing and markers oscillating for arm trials.

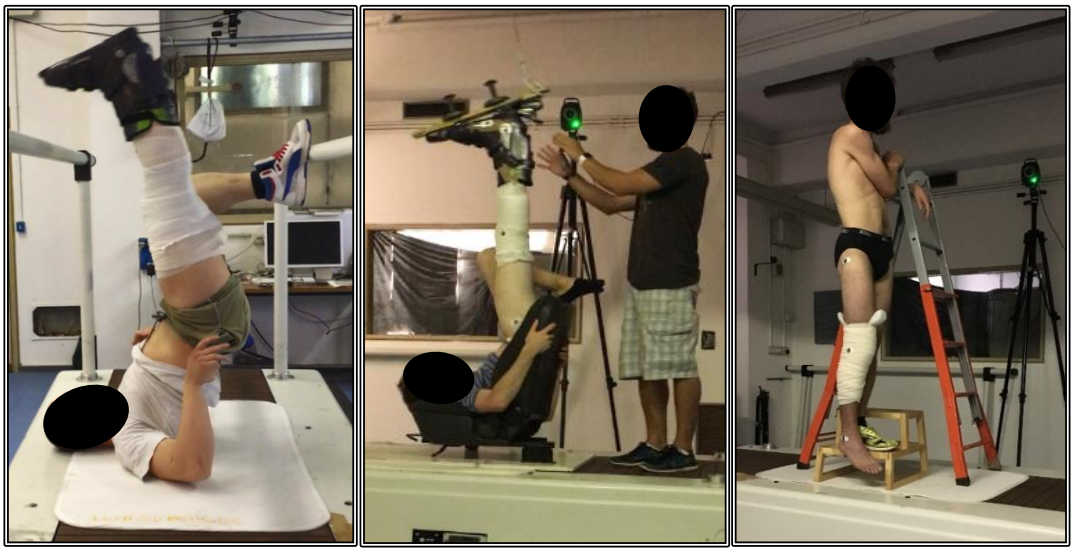

Figure 16. (left) First subject to attempt cast integrity for inverted trials. (middle) subject leg fitted with a second cast swings with additional load but insufficient leg range of motion. (right) subject fit with a previously removed cast shows fitting and integrity issues which don't allow for loaded testing.

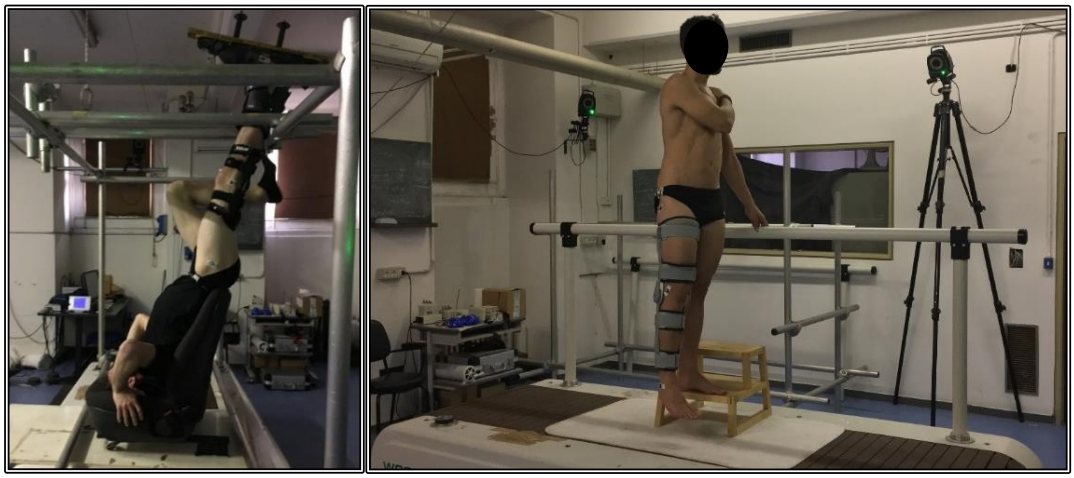

Figure 17. (left) An inverted subject is tested with the small brace which allows for marker placement. (right) The final brace is shown on a subject in the straight, unloaded position. Subject hold the rail with left hand while keeping right hand from occluding markers.

Limb loading

Investigating the damping in oscillating limbs under compressive loading requires a system for attaching loads to the limb. The originally proposed solution was to load to the limb distally, using a rigid ski boot attached to modified skis where the additional masses could be added (Figure 18). Mismatched boot and foot size led to undesired auxiliary movement in most subjects. Additionally, attaching the masses at such a distance from the axis of rotation lead to a very large moment of inertia making it very difficult to create a reliable push of the leg. The final brace which was chosen offered a solution to both issues. Since there are metal supports running the medial and lateral length of the brace, it allowed for the additional masses to be secured directly to the brace (Figure 19). Attaching the masses directly to the limb prevented additional movement of the masses during limb oscillation. It also allowed for the heavier masses to be attached proximally and lighter masses to be attached distally effectively resulting in a smaller moment of inertia.

Postural support

Applying a load to the lower limb of a subject required using a 'chair' which could securely support an inverted subject while allowing ample range of motion (ROM) of the limb. The first proposal was to use a seat from a car which frequently resulted in either obstructed limb ROM because the hip joint does not rest above the seatback (Figure 16), or full ROM with the subject exposed to cervical spine loading (Figure 17). The solution was to construct a chair with an adjustable seatback height and a gap for the head to pass through (Figure 19). In this setup, the load is supported by the shoulders and the seatback can be raised or lowered for each subject.

Figure 18. Ski boot attached to modified skis for applying additional load.

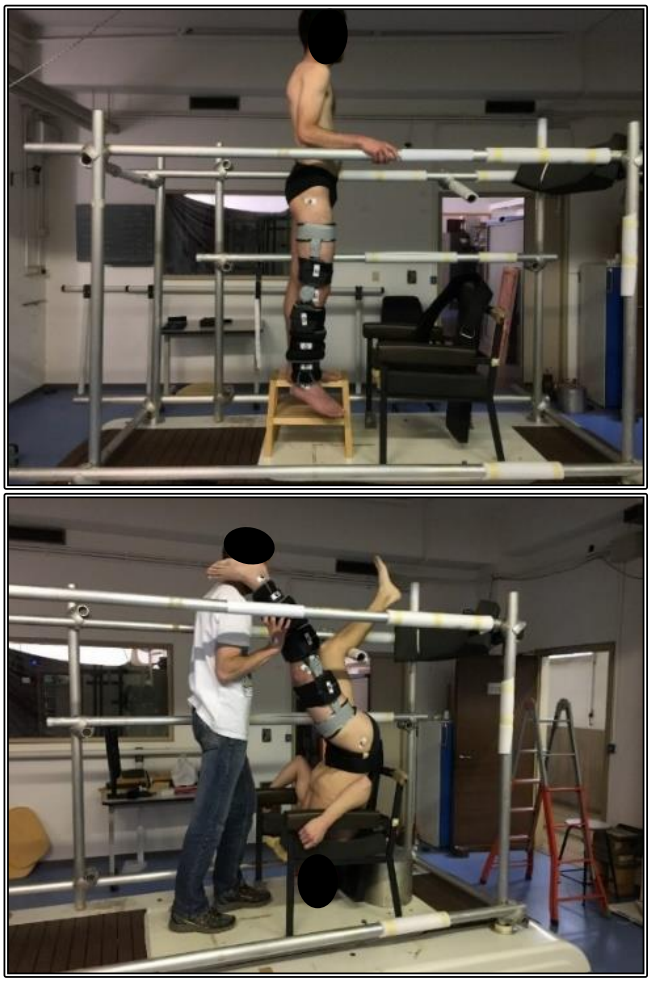

Figure 19. Subject with loaded limb in the upright position (top) and the inverted position (bottom).

Methods

Experiments were performed on the upper and lower limbs of sixteen males (age 26±3 years; height 1.79±0.08 m; body mass 73.0±6.7 kg; mean ± SD) who were tested in a series of 7 trials, each with 10 repetitions. The trials were: straight unloaded upper, and lower limbs oscillations, inverted unloaded, inverted loaded with loads of +4, +8, +10, and +12kg. In the upper limb trials subjects were asked to remove their shirt or wear a loose fitting shirt as to not impede limb oscillations. In the lower limb tests, the subjects wore underwear to allow for free limb oscillation as well as applying reflective markers to the skin. Limb oscillation kinematics were sampled at 200Hz using a 7 camera infrared motion capture system (VICON, United Kingdom) with the following limb and load specific methods.

Straight upper limb

Subjects were fitted with three reflective markers on the shoulder, elbow and hand. A rigid rod was fixed to each subject's right upper limb to block elbow flexion. Subjects were then seated and asked to lean laterally over the right side of the chair so that their arm could hang and oscillate freely, without contacting the chair or ground. An operator would then lift the subject's hand, hold it in place momentarily, and release the arm to oscillate freely until brought to rest by the internal damping. Numerous familiarization swings were performed until the subject was able to allow his limb to oscillate freely, at which point the recorded tests were initiated. The subject's arm was tested until ten valid tests were collected. A test was repeated if the subject's limb touched anything else or if oscillation was obviously affected by the subject.

Straight lower limb

Each subject was fitted with three reflective markers on the hip, knee and ankle joints. A full-length leg brace was adjusted to properly fit to each subject according to their leg length and circumference. The subject was asked to stand on one leg atop a small platform which then allowed the contralateral leg to be studied as it freely oscillated. The subject would lean slightly to the side of the swinging limb to prevent it from contacting the small platform. Balance was maintained with one hand by holding a rail while being sure to keep the other hand free from occluding the view of the reflective markers (Figure 17). Similar to the upper limb, an operator would lift the subject's foot, hold it in place momentarily, and release the leg to oscillate freely until brought to rest by internal damping. Numerous familiarization swings were performed until the subject was able to allow his limb to oscillate freely, at which point the recorded tests were initiated. The subject's leg was tested until ten valid tests were collected. A test was repeated if the subject's limb touched anything else or if oscillation was obviously affected by the subject.

Inverted lower limb

Since the swing of the inverted limb is now required to overcome gravity, an impulsive acceleration must be applied to the subject's limb by an operator. The ideal push was not intended to swing the limb quickly over the subject, but rather accelerate the limb just enough to overcome the negative acceleration due to gravity and allow the limb to fall softly to the opposite side. After the acceleration was applied, the limb was left to freely rotate about to subject's hip joint until coming to rest on the padded safety structure surrounding the subject. In addition to the markers already placed on the leg, a marker was placed at the center of each additional load to track its location, and on the hand of the operator to know when

the limb was released to oscillate freely. To begin, the subject was assisted to enter the chair and lift his leg to load the joint. Once in position, multiple familiarization tests were done by incrementally increasing distances that the leg would swing. First the limb would be moved back and forth while the operator constantly held the leg. Then the leg would be softly dropped on the support structure. Finally, a full push was performed allowing the leg to swing and fall onto the support structure. This was done until the subject was able to perform the swing without inhibiting the limb oscillation. At which point, the recorded tests were initiated and repeated until ten suitable tests were collected in each loading scenario. If the limb did not complete a full swing or was impeded in any way, the trial was discarded and repeated. The loading scenarios started with 12kg and decreased incrementally (10kg, 8kg, 4kg) by always removing the most distal load until the final tests were completed without any additional load. Once each loading scenario was completed, the subject was assisted to exit the chair and given a brief period to rest and stand upright while the load was removed before moving to the next series of tests.

Data Analysis

To evaluate the additional positive work required to overcome the internal damping of limbs during oscillatory movements, it is important to consider each limb individually since their interactions with the environment vary between joints and across locomotory phases. The shoulder experiences only tensile load during bipedal locomotion, regardless of the swing or stance phase. Meanwhile, the hip alternates between tension and compression. To find the damping within each limb requires distinctly different approaches depending on the loading of the limb. For both the upper and lower limbs in the straight position, under tensile load, the limbs are able to oscillate which allows for an exponential fitting of the oscillatory peaks. The inverted lower limb provided only one oscillation and required a much more involved data analysis.

The behavior of viscously dampened oscillators can be represented as a sin wave with and initial amplitude (A) which is steadily decreased by the damping force (B) within the limb and a frequency (C):

$$\theta(t) = Ae^{-Bt}Sin(C)$$

After accounting for the physical properties of an oscillating limb, $A, B, \& C$ are replaced to give the limb specific damping equation developed in the math model:

$$\theta(t) = Ke^{-\left(\frac{A}{2}\right)}Sin(\omega t + \emptyset)$$

Using this approach, the first step to calculating the friction (damping) within the limbs required finding the exponential decay of the of each subject's oscillating limbs.

Straight upper and lower limbs

The exponential fit, $y = pe^{qt}$ to the peak oscillation displacements shown in Figure 20 have an exponential decay, q of -0.34 which if applied to a sin function starting at the amplitude 0.691 radians, would result in the respective graph of the experimentally captured data. However, in an oscillating limb, the decay of -0.34 is comprised of more than just a unitless number. The damping q is represented by $\left(\frac{A}{2}\right)$:

$$q = \left(\frac{A}{2}\right)$$

And A as defined in the math model is equivalent to $\frac{b}{m\,R_g^2}$ where b is the actual, limb specific damping:

$$b = 2mR_g^2 q$$

For example, a limb which oscillates as in Figure 20, with a m of 3.3kg, and a $R_g$of 0.368m, would have a viscous frictional damping force of 0.303 $N \cdot m \cdot s \cdot rad^{-1}$. This process as performed for every valid trial of each subject to find the mean viscous damping of each subject's upper and lower limbs and then compared depending on the tensile load due to the mass of each subject's limb. As shown in Figures 20 and 21, the oscillating upper and lower limb could often exhibit quite similar starting amplitudes and, in some cases, even exponential decay. However, after equating for m and R_g of each limb, the value of the frictional coefficients can be quite different. The lower limb in Figure 21 has a similar starting amplitude exponential decay as the lower limb in Figure 20. But with a limb mass of 10.626kg, and R_g of 0.469m, the damping of the lower limb is much higher, $b = 1.956\ N \cdot m \cdot s \cdot rad^{-1}$

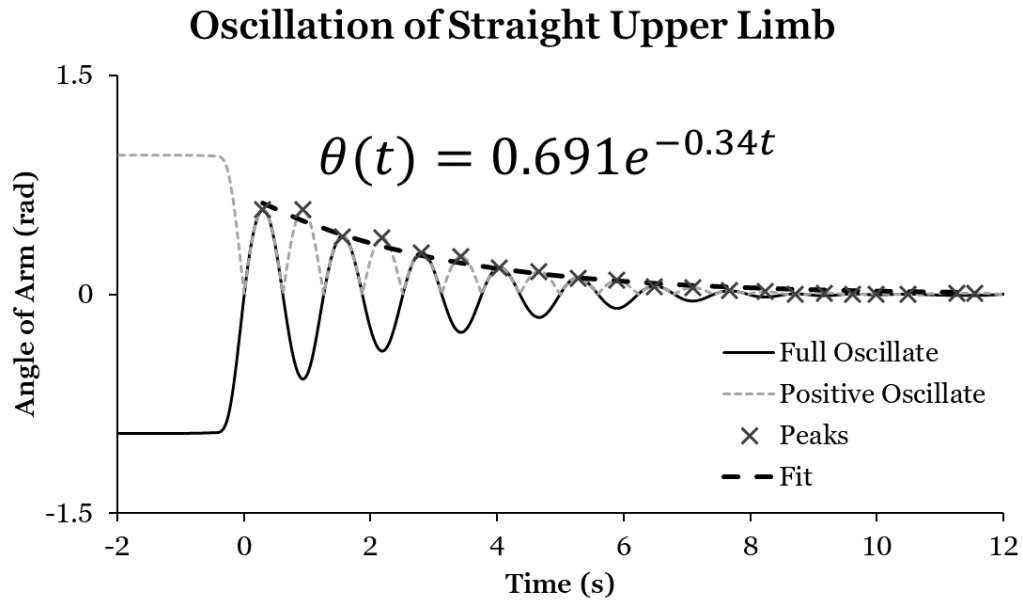

Figure 20. Oscillation of straight upper limb with positive rendered values and an exponential curve fit to the max angular displacements.

.

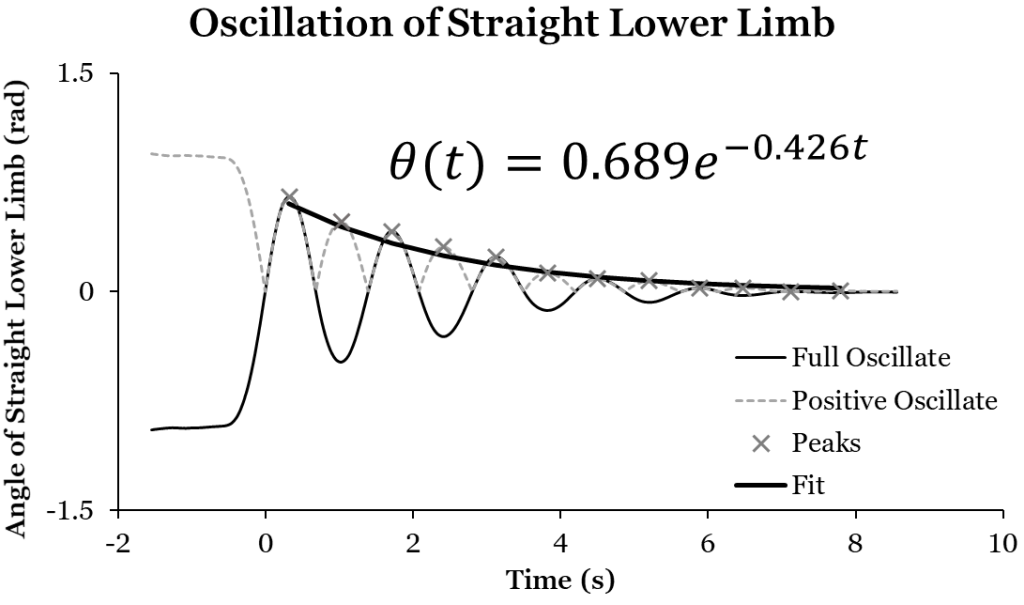

Figure 21. Oscillation of straight lower limb with positive rendered values and an exponential curve fit to the max angular displacements.

Inverted lower limb

The computation of loaded lower limb damping was decidedly more intricate. Since the inverted position did not allow for multiple swings, an exponential decay could not be used. Rather, the dynamics of a single swing had to be used to determine *b*. Utilizing the limb dynamics required building a custom software package (LabView, National Instruments, US) which worked in three stages. The three stage process was repeated for every inverted limb test of every subject. The first stage was to repetitively run and observe the phase plane of the center of mass (COM) of the limb and all attached masses. Doing so, allowed us to trim the data of each test so that the largest dynamically unaffected portion of the swing was analyzed (Figure 22). Trimming the data also provided the effective start and end points of each swing. Those data points were then input into the second stage of the data analysis software to find the corresponding damping which would result in the same trajectory.

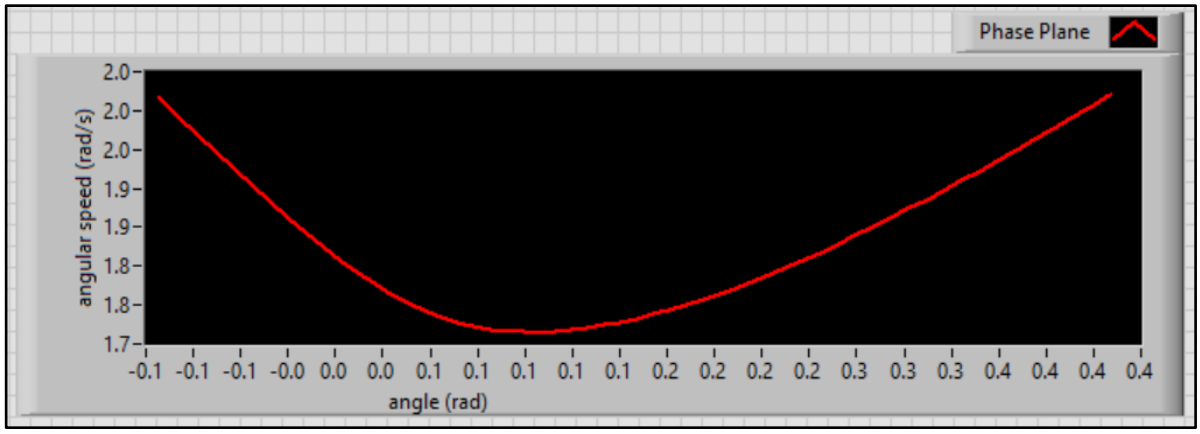

Figure 22. A diagram of the first stage of the program interface used to inspect and trim the phase diagrams of the inverted limb oscillations in order to determine the initial and final conditions of the limb COM.

The second stage of the data analysis required all of the initial and final conditions; θ_0, θ_{end}, $\dot{\theta}_0$, and $\dot{\theta}_{end}$ provided by the first stage plus the R and R_g found separately. Using these inputs, the routine would iteratively provide curves based on the starting inputs (Figure 23) and a user defined range of b values (Figure 24). It would also provide a 'goal' where the curve should terminate based on the experimentally gathered final conditions.

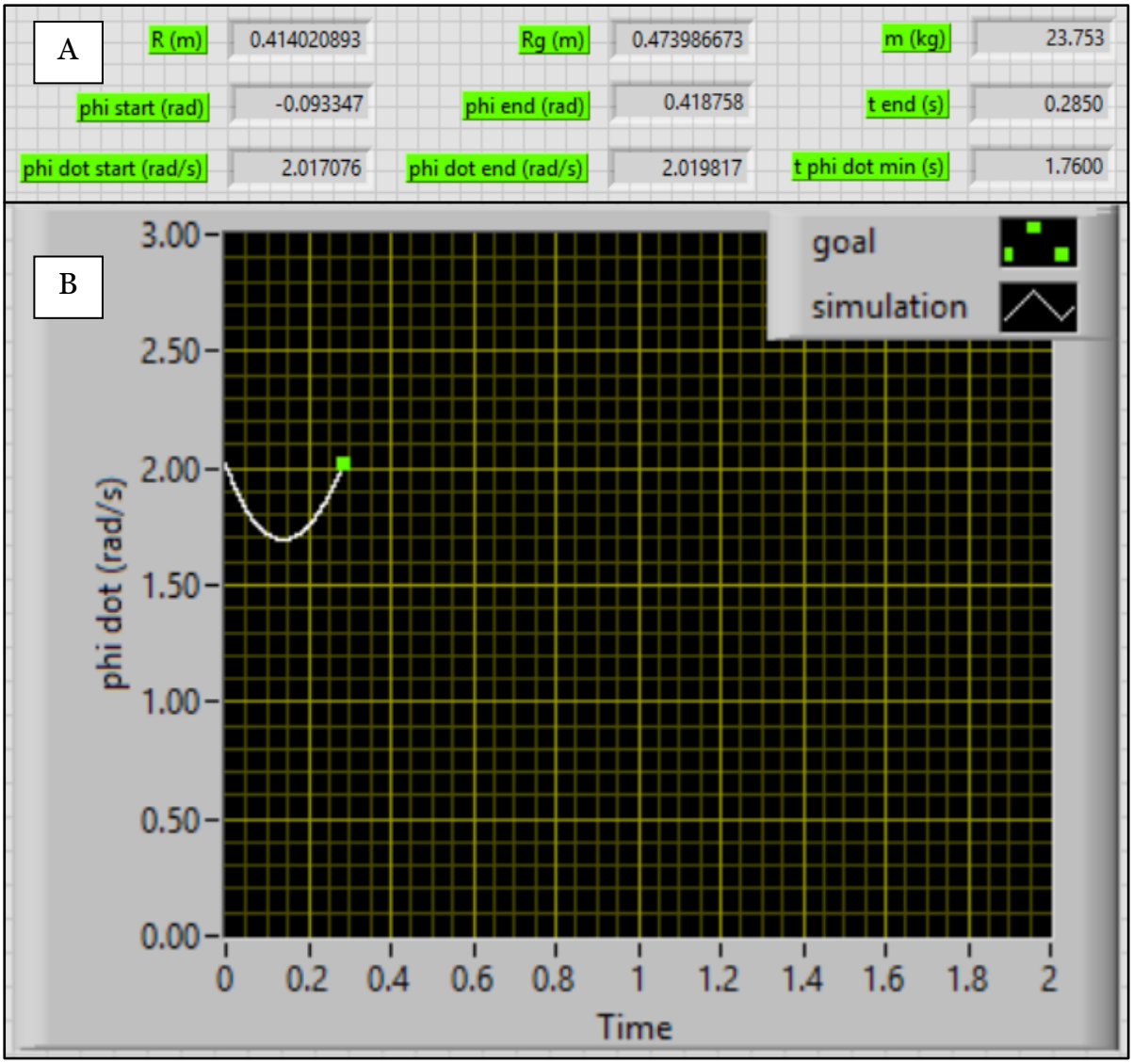

Figure 23. A) Input values determined in first stage. B) Simulated plot of a curve base on the initial conditions of the system and the imposed range of b values (white line), and the goal of where the curve should terminate based on the experimentally collected final conditions (green dot).

Once a valid range of *b* values was able to provide a curve which both initiated and terminated within a given threshold of the experimentally determined θ_0, θ_{end} and $\dot{\theta}_0$, $\dot{\theta}_{end}$, the *b* range could be incrementally refined, and the damping simulation rerun until the most precise range of damping values (lowest n) was determined (Figure 24).

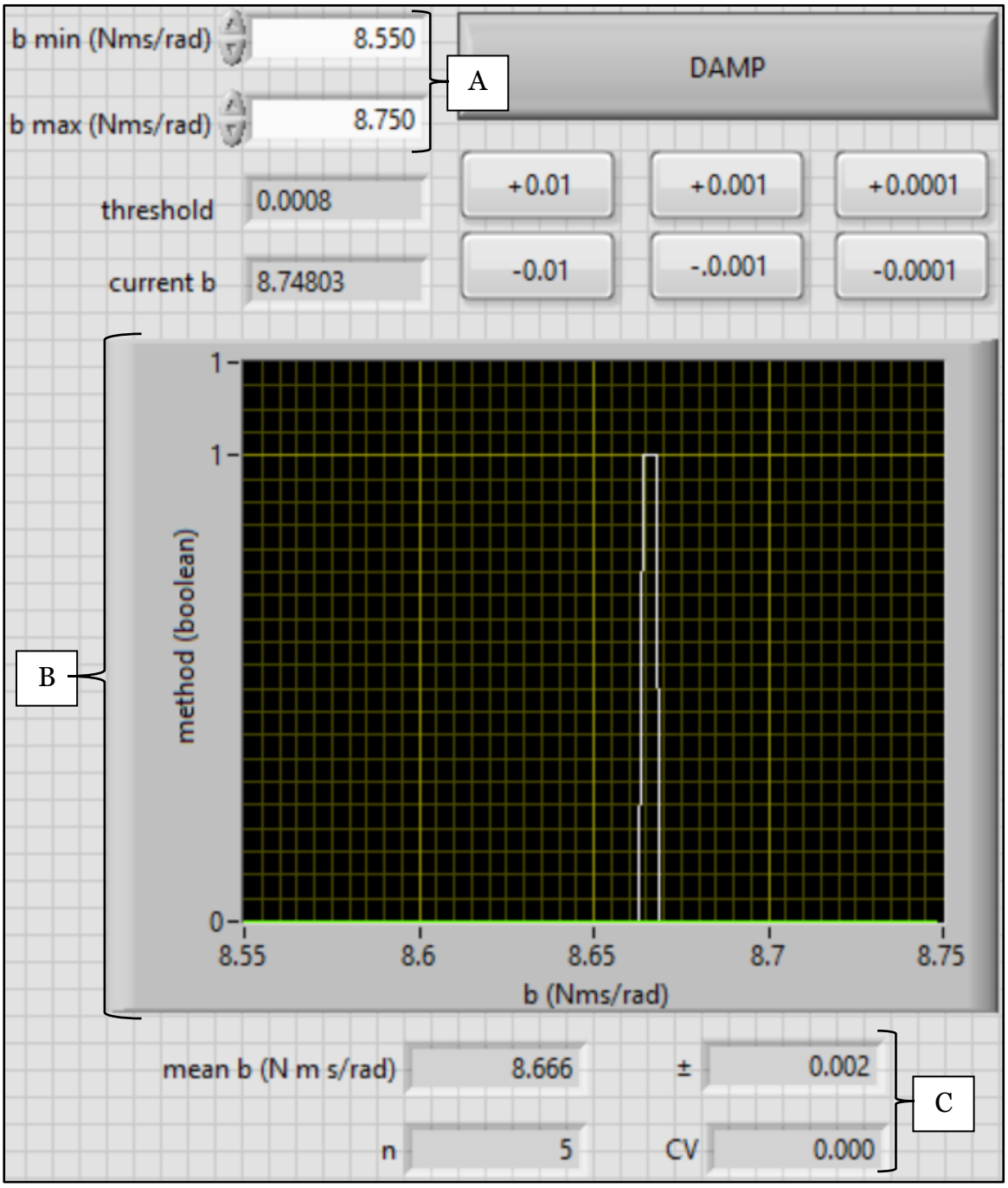

Figure 24. A) User defined *b* value range. B) Graphic representation of *b* values which create curves with end points within the given error threshold. C) Mean, SD, n and CV of found *b* values.

Results

Straight upper and lower limbs

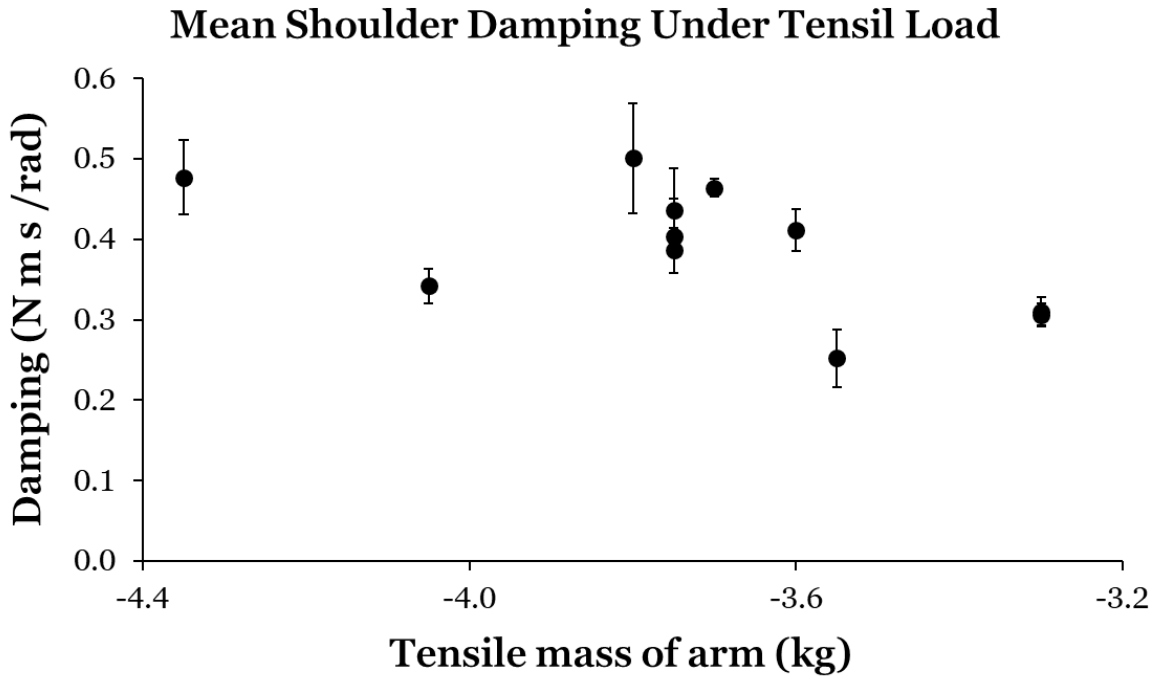

Figure 25. Mean ± SD of upper limb damping for each subject in relation to the tensile mass of the subject's upper limb.

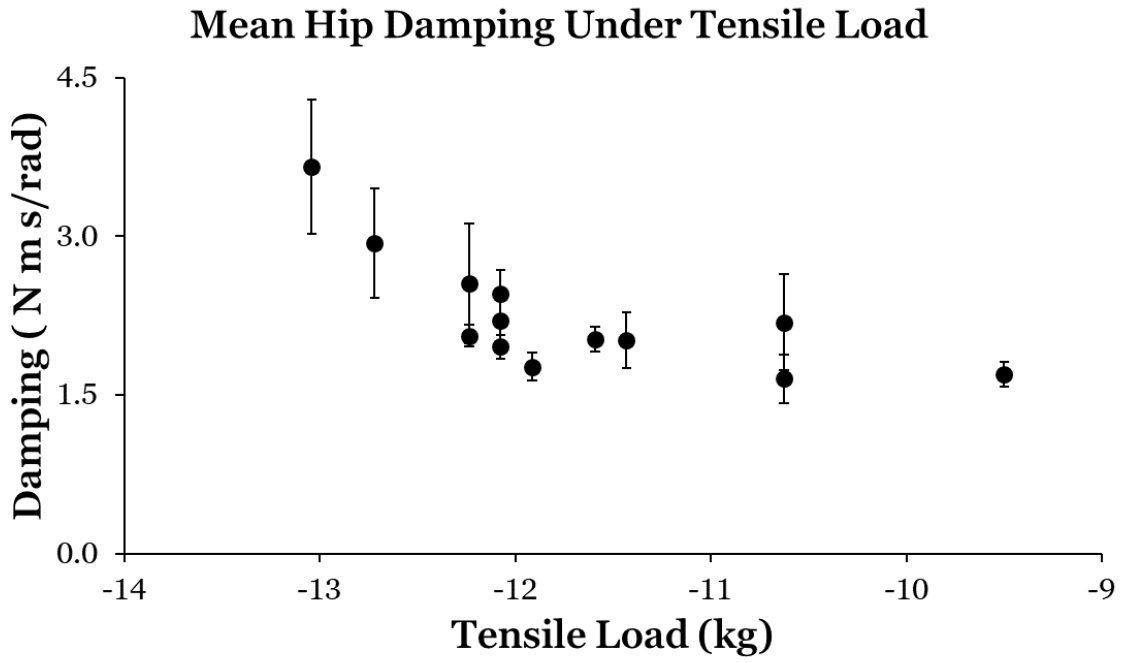

Figure 26. Mean ± SD of lower limb damping for each subject in relation to the tensile mass of the subject's lower limb.

The mean ± SD viscous upper (Figure 25) and lower limb (Figure 26) damping values of all subjects who completed the straight limb tests are plotted in relation to the tensile load of the subject's limb. Since there were no additional loads in the straight tests, the subjects load was constant for each subject and the subjects were not grouped. The difference in mass was less than 1kg for the upper limb and less than 5kg for the lower limb across all subjects. Mean tensile upper limb damping was b_{UU} = 0.39 ± 0.08 N m s rad^{-1}. Mean tensile lower limb damping was b_{UL} = 2.24 ± 0.56 N·m·s·rad^{-1}.

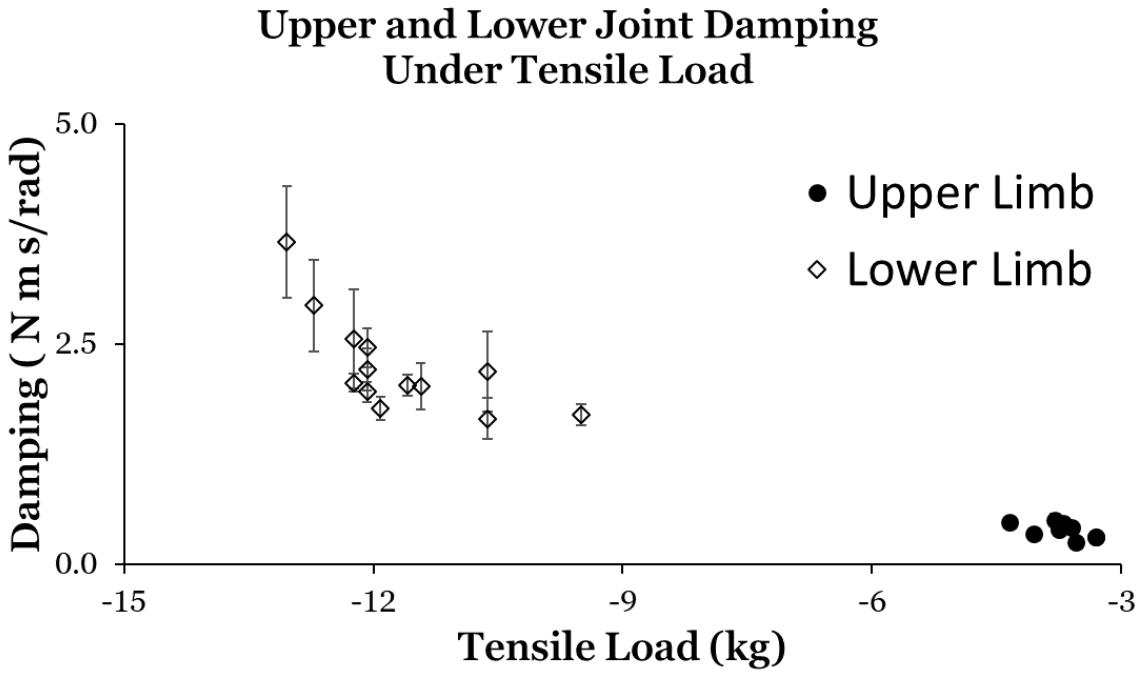

Figure 27. Mean ± SD of the lower and upper limb viscous damping values in relation to each other. As seen, the SD of the lower limb values are much greater, whereas, with the upper limb, SD values are so small that they do not extend beyond the symbols for mean value.

A great difference between the upper and lower limb damping can be observed in the grouping of the *b* values (Figure 27).

Inverted lower limb

Since additional loads were added to the inverted lower limbs, the subjects were grouped by added mass to more effectively compare the differences in lower limb damping. The joint load values were divided into groups according to the added mass (leg only, +4kg, +8kg,+10kg, +12kg).

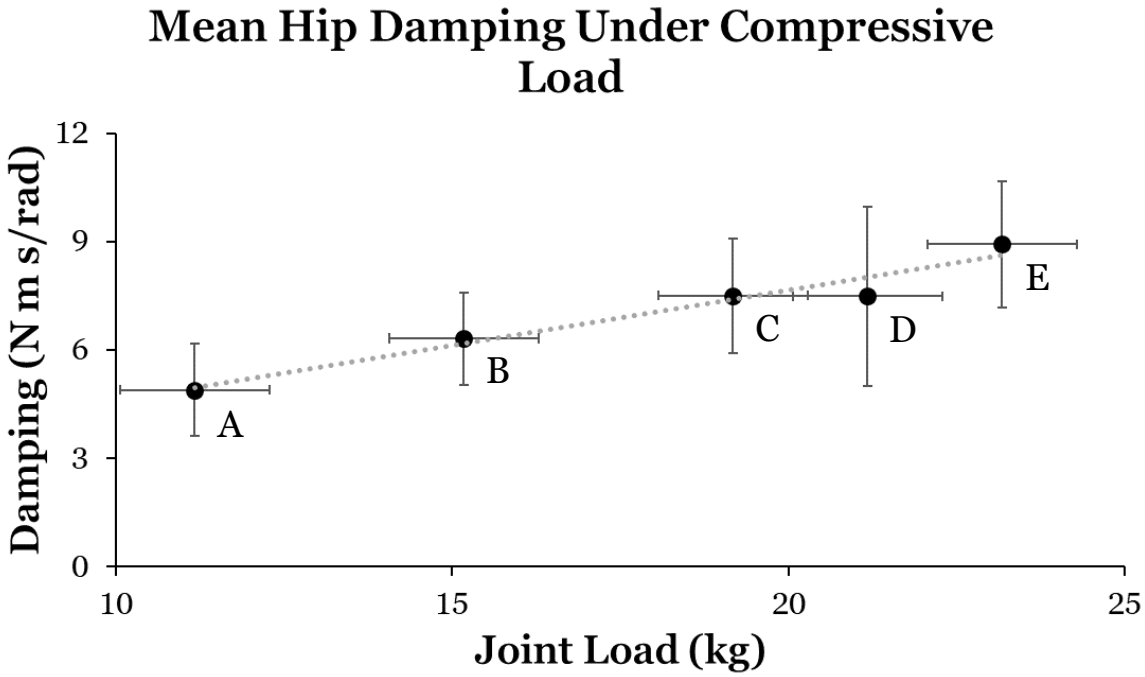

Figure 28. Mean ± SD of lower limb damping for each subject in relation to the compressive mass of the system. A) leg only B) +4kg C) +8kg D) +10kg E) +12kg

As full body mass varied across subjects, so did the respective limb masses and the mean load of each group. Therefore, the SD of joint load across groups was a result of the anthropometric variance amongst the subjects (Figure 28).

Overall damping

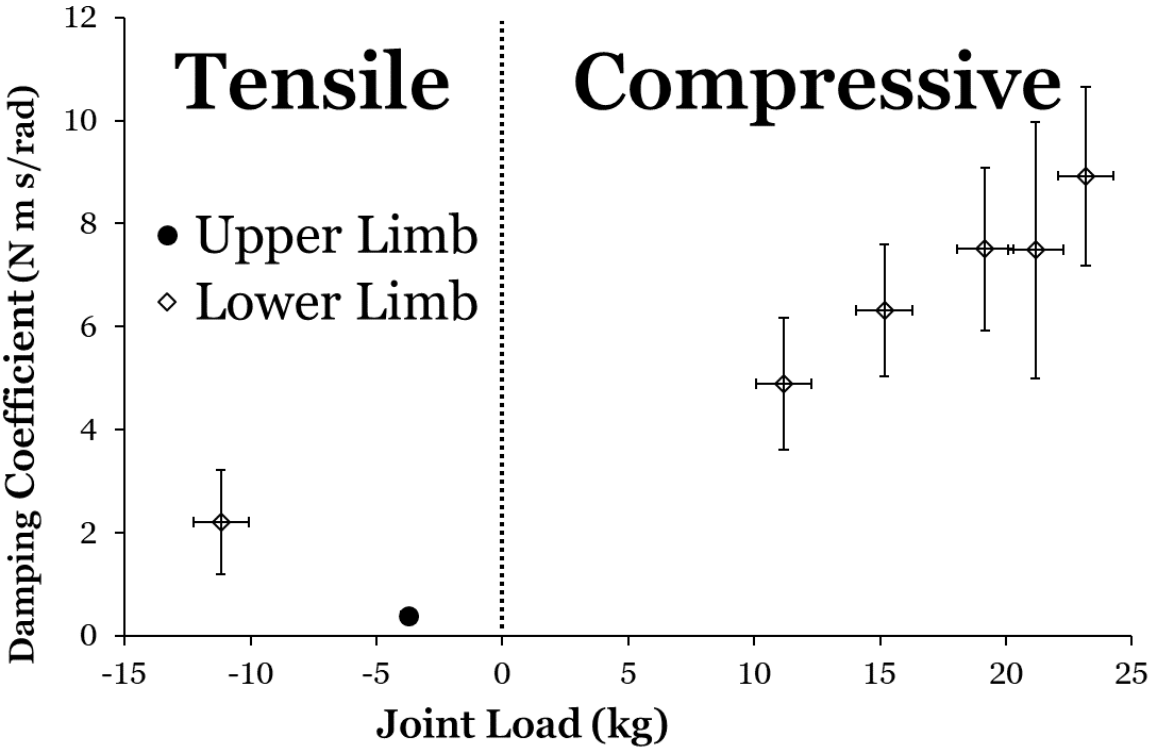

Figure 29. Comprehensive graph of all damping coefficients calculated for the upper limb (closed circle) under tensile load and lower limb (open diamond) under both tensile and compressive load. As seen in Figure 27, the SD of the upper limb damping is once again so small that the error bars are hidden by the mean value symbol.

When observing the overall damping within limbs (Figure 29), it can be seen that in both tensile and compressive scenarios, increased load leads to greater damping.

The estimate of the internal work due to friction (damping) can be obtained by using equation 46 with the damping factor measured during the illustrated experiments (maximum b factor for the loaded lower limb). The final predicting equation ($C_{mif}, J\ kg^{-1}m^{-1}$) is:

$$C_{mif} = 0.24\bar{v}$$

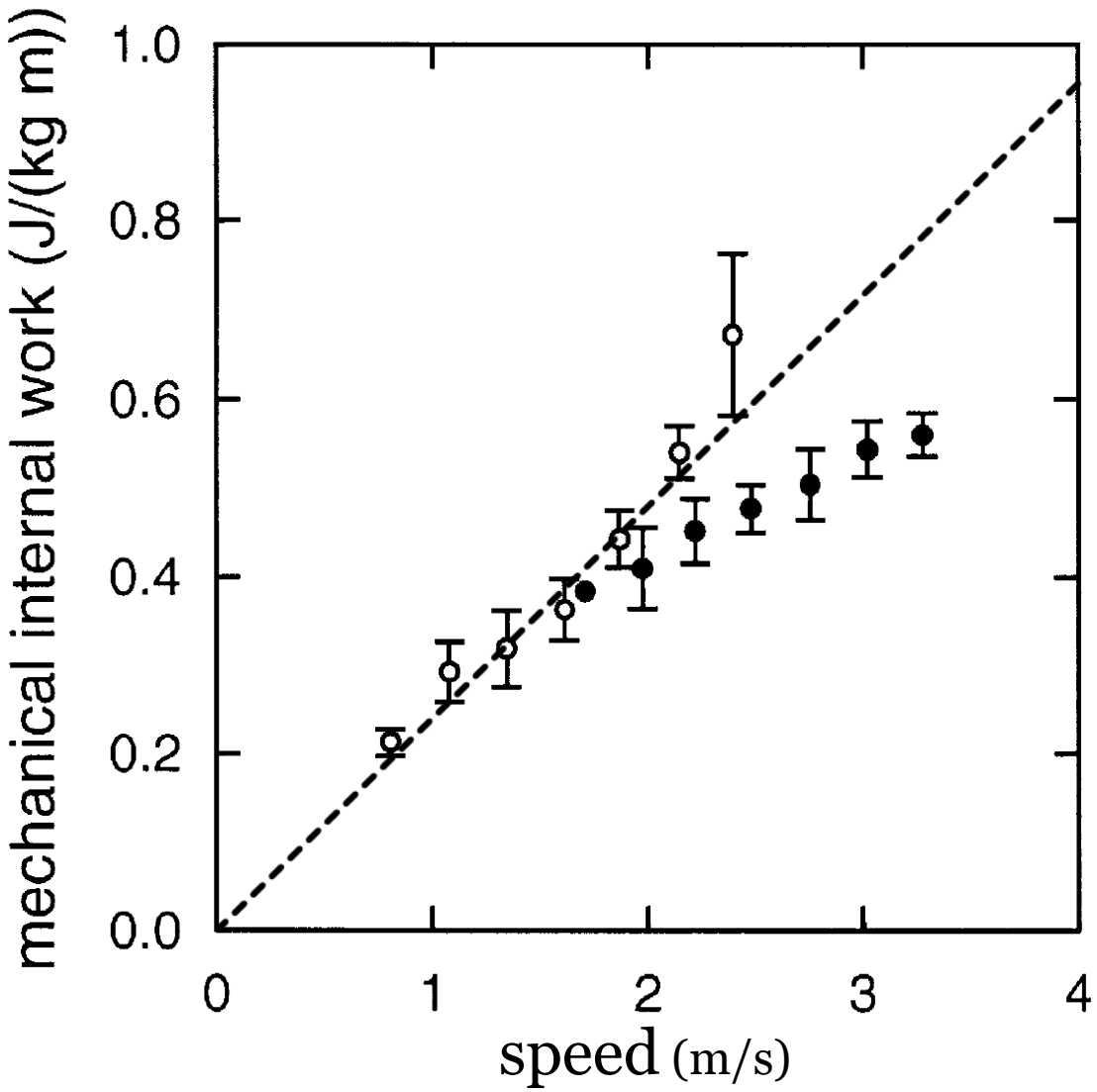

Figure 30. The mechanical internal work due to friction (damping) according to the predicting equation $C_{mif} = 0.24\bar{v}$ (dashed line) at different speeds charted over the total mechanical work of walking (open circles) and running (closed circles) at various speeds found by Minetti (1998).

Figure 30 shows the mechanical work due to friction (damping) according to speed and is plotted along with the internal work due to running and walking to see a comparison between the three.

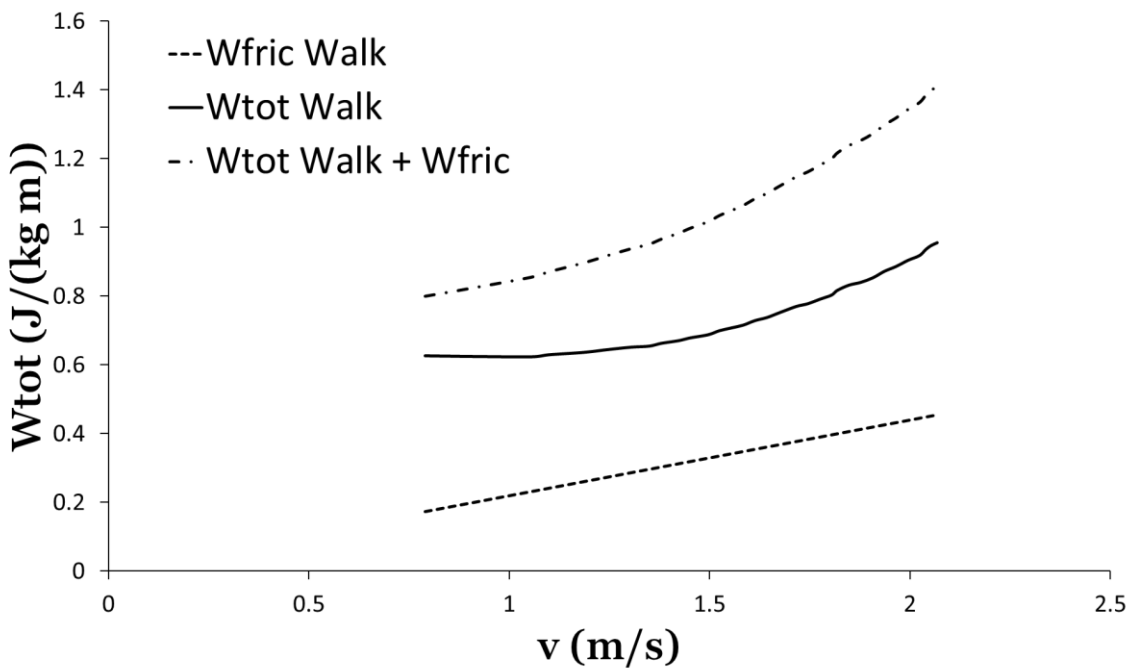

Figure 31. Plot of mechanical work during walking. The dotted line is the work due to friction according to the predicting equation $C_{mif} = 0.24\bar{v}$. The solid line is the total work of walking without the work of friction. The interrupted line is the mechanical work of walking including the work due to friction. Data adopted from Pavei (2014).

At the optimal speed of walking (1.4 m/s), C_{mif} quantitatively corresponds to about 25% of the sum of the 'kinematic' internal work ($W_{INT,KINE}$) and external work (W_{EXT}) as can be seen in Figure 31. It is also important to notice that since C_{mif} is speed dependent, the $W_{TOT} + W_{INT,FRIC}$ does not just result in an upward translation, but also a change of slope.

Discussion

The aim of this thesis was to understand if there could be damping due to friction within human joints while the limbs swing during locomotion. In order to measure the damping, two different setups were utilized; one resembling the unloaded swinging limbs and the second, the stance phase with loaded swinging lower limbs. By observing the time course of passive upper (Figure 20) and lower limb (Figure 21) oscillations, internal frictional damping (b, N·m·s·rad^{-1}) has been shown to be present in both limbs. Phase planes of the oscillation cycles (Figure 13) were used to confirm that the limb oscillations were unaffected by muscular activation from the subject, meaning that the energy dissipation was due solely to internal damping. Using the maximum angular displacements of the successive swings an exponential decay was determined. A custom developed 2nd Order Non-Linear Ordinary Differential Equation allowed the friction (damping) coefficient b to be inferred from the exponential decay. Upper limb damping ($b_{UU} = 0.39 \pm 0.08$) was found to be approximately six times lesser than lower limb damping ($b_{UL} = 2.24 \pm 0.56$) during the swing phase. Since the two joints are very different it is difficult to speculate whether the increased tensile load of a larger lower limb can explain the higher damping coefficient or if the difference can be simply due to different joint structures. Without an additional compressive load, internal damping should be attributed solely to a subject's physiological traits such as the viscosity of their synovial fluid, smoothness of articular cartilage, surface interactions between muscular tissue, fat tissue, and skin, and the many other internal tissue interactions which take place during movement. The lower limb, however, does experience loading during the stance phase and therefore required added load in the inverted position to simulate load bearing during walking. Since added loads may lead to

deformation of the tissues it was expected that the friction experienced within the joints was non-Newtonian, and higher loads would lead to higher damping. Inverted limbs under compressive load showed a proportional increase between the limb loading and damping factor (Figure 28). Mean lower limb damping under the highest experimentally tested compression (118 N) was 8.92 ± 1.74 Unfortunately, due to constraints of the experimental setup, loads equivalent to that of the physiological load during locomotion were unable to be tested. Despite the seemingly observable linearity of the *b* values, it must be remembered that each point is derived from the processing of one, single swing (rather than multiple oscillations as in the upper limb) which comprises a small portion of a circular trajectory, and that often the adhesion to this model was problematic. The large discrepancy between the added load (approximately 23 kg, including the mass of the leg) achieved experimentally and that experienced during locomotion (≥50 kg) does not allow a safe evaluation of the damping value, future studies should overcome present constraints to reach locomotion values. This study has shown that damping is present with both the upper and lower limbs under tensile load and in the lower limb under compressive load. Approximately 93% of the damping in limbs during locomotion is attributed to the lower limb, 75% of which is during stance. Only 7% of damping is due to upper limb damping, both during the swing and stance phase.

As previously discussed, the primary aim of this thesis was to estimate the damping coefficient due to damping within limbs during the different phases of locomotion. Subsequently, those values could be incorporated into the mechanical works of locomotion to provide a more complete vision of the comprehensive locomotor needs. Prior studies have proven and measured the existence of friction within sacrificed animal joints (Jones 1934, 1936; Charnley, 1960; Crisco 2006). However, the studies often excised the surrounding tissues (Barnett and Cobbold, 1962;

Unsworth et al., 1975a, 1975b) resulting in frictional damping values which are less than those in an *in vivo* human joint. Furthermore, the values were never applied to the energetics of locomotion. The results from this study have confirmed and quantified the amount of damping which is present *in vivo*; not only in each limb but also in each phase (swing and stance) of locomotion. With these values, it is possible to consider their effects on the locomotive system as a whole.

The total mechanical work of locomotion is traditionally defined as the sum of the work done to raise and accelerate the body center of mass within the environment, External Work, and the work done to accelerate the limbs in relation to the BCoM, Internal Work. Of the two, W_{EXT} is considered to be less problematic regarding its quantification as it can be done by tracking the trajectory of BCoM (Margaria,1976). This has been validated in multiple ways (Fenn, 1930; Cavagna et al. 1963, Cavagna,1975; Pavei et al., 2017) but there can be some sources of error such as 'external' resistances from air resistance when moving outside without a tailwind. Additionally, the 'apparent' external work can actually be slightly less than that measured due to elastic energy which stored within the tendons and is returned to the system during takeoff and therefore reduce the W_{EXT} done by the muscles (Fukunaga et al., 2001; Minetti, 2004). This is most apparent during bouncing gaits (Margaria, 1976; Blickhan, 1989; Minetti, 1998b) but also seen in walking (Peltonen et al., 2013; Maganaris and Paul, 2002). In contrast, the evaluation of W_{INT} is more complex and has been considered in many different ways during the course of locomotive research (Fenn, 1930; Cavagna and Kaneko, 1977; Minetti and Saibene, 1992; Minetti, 1998a). Fenn (1930) was the first to attempt measuring the additional work required to accelerate the limbs about the body. He did so while also making the first mention of internal friction. His perspective of friction was focused only

within the muscles that should have been the cause for muscle efficiency, which he then found to be negligible. This approach to measuring the kinematic work of reciprocal limb movements was valuable in establishing a framework for what was later adopted by Cavagna et al. (1963) utilizing König's theorem that partitioned W_{TOT} into W_{EXT} and W_{INT}. This method was later refined by Cavagna and Kaneko (1977). König's theorem can be considered correct in the division of kinetic energies (KE). Total kinetic energy (TE) is equivalent to the sum of the KE of BCoM (which is included in W_{EXT}) and the rotational KE of the limbs (the proper W_{INT}). However, it is questionable to divide the effect of the W_{EXT} from that of W_{INT} because the separation of the two seems to negate the energy saved due to the ballistic movements of the oscillating segments (Alexander, 1989) and would result in an over estimation of the W_{TOT}. Despite the successful use of the $W_{EXT} + W_{INT}$ method in relation to the metabolic cost of locomotion in various gates and conditions (Minetti, 1993; Minetti, 1994), criticism began appearing.

One of the first methods presented in opposition to the $W_{EXT} + W_{INT}$ method was that suggested by Winter in which all of the negative and positive work is summed resulting in an implausible amount of work (1979). This was followed by Aleshinky who wrote a series of papers (1986a, 1986b, 1986c, 1986d) in which he lengthily deconstructed and refuted the $W_{EXT} + W_{INT}$ method, as well as Winter's method (1979) and brought forth his own alternative. However, the alternative offered by Aleshinsky required numerous unresolved assumptions and lead to unreliable results. Years later, a criticism was written by van Ingen Schenau (1990) in which he also proposed a very detailed rendering of power equations about the joints. This method had theoretical and practical limits based on the distance that measurements were taken from the joint centers.

There is one common variable missing from all of these methods. The energetic dissipation of friction within the body (such as that experienced at the joints) is irrefutable. Each time that energy is expected to be dissipated by friction within joints, there must be an equivalent energy supplied by the muscles to overcome that deceleration and maintain the oscillation of the limbs without slowing. In order to have a more complete understanding of W_{TOT} it is necessary to measure the work required to overcome friction ($W_{INT,FRIC}$) during the cyclical movement of the limbs. And yet, even with the numerous different approaches to calculate the mechanical work of locomotion, as of now, they all only measure the work associated with the kinetic movements $W_{INT,KINE}$; leaving $W_{INT,FRIC}$ yet to be measured. One somewhat particular experiment which could be done to illustrate the paradox between the roles of $W_{INT,KINE}$ and $W_{INT,FRIC}$ would be: if a subject was asked to mimic the ideal pendular oscillations of the lower limb, the mechanical result would be $W_{EXT} = 0$ and $W_{INT,KINE} = 0$. But this would not reflect the work actually being done by the muscles, which to imitate the *passive* pendulum, in fact, should *actively* overcome the damping of the limb. In this case, therefore, only $W_{INT,FRIC}$ would indicate the work effectively done by the subject.

As shown in many experiments (Cavagna et al., 1963, Cavagna et al. 1964, 1976; Cavagna and Kaneko, 1977; Winter, 1979; Williams and Cavanagh, 1983; Minetti, 1998a; Minetti, 2003) W_{EXT} is not sufficient to explain the metabolic energy cost of locomotion. The summation of W_{EXT} and W_{INT} (not considering $W_{INT,FRIC}$) when calculated independently, can function to set an upper limit (W_{TOT}; no energy transfer between W_{INT} and W_{EXT}) of the predicted metabolic energy spent to move in accordance with each individual task and environment; whereas when considered mutually by adding the time courses of BCoM and the segmental energies, and then

summing the increases in the resulting curve, a lower limit can be set (W_{TOT} $*$; best possible energy transfer) (Minetti, 1999). In cycling, W_{TOT} is only correct if W_{INT} is considered proportional to the frequency of pedaling (Francescato et al., 1995). Yet, in a study by Minetti (2011) using a physics simulation program (Working Model 2D, Knowledge revolution, USA) it was shown that regardless of load or frequency, a frictionless system could spin forever with no additional energetic drive to maintain motion after an initial energy was provided to the system. This demonstrated that the kinetic internal work of cycling to maintain pedaling rotation is, in essence, zero or negligible. Yet, it has been confirmed that as cycling cadence increases, so too does metabolic consumption (Francescato et al., 1995). The discrepancy between these two findings seems to indicate a sort of internal 'viscous' work done to overcome damping within the musculoskeletal machinery, which coincidentally coincides with the theoretically non-existent $W_{INT,KINE}$ (Minetti, 2011). With the present data, we can attempt to answer the question: Is internal viscous damping truly responsible for the additional metabolic consumption? And is that applicable not only to cycling but also walking, running, skipping, etc.?

For walking, the curve $W_{INT,FRIC}$ is nearly superimposable to that established by Minetti (1998) of $W_{INT,KINE}$ (Figure 30). In cycling, this would require a separate tailored equation in which the *b* factor should additionally include the friction within the knee and ankle measured with average loads. In locomotion, other than cycling, with the pendular movements of the four limbs, we cannot hypothesize that $W_{INT,KINE}$ is inexistent (as in cycling) and $W_{INT,FRIC}$ cannot be quantitatively substituted but should rather be added to W_{TOT}. There are some factors, such as the reciprocal movements of the limbs, which may lead to an underestimation of $W_{INT,KINE}$, and other factors, such as the passive nature of the swing and stance phase in which

slowing is required even of those structures which should normally be active; the muscles which sustain the cyclical movement.

This apparently unprecedented work for the applications in the locomotor mechanics opens the door to multiple specific activities. Where the rotational damping was never previously considered, it can alter the previously understood mechanic and energetic ratio (estimated muscular efficiency). The ratio which, without elastic contributions, should not exceed 25-30% (Woledge, 1985), could now, given the addition of friction, increase and reveal elastic contributions to gaits in which they were previously thought to be negligible or nil.

The estimated frictional damping values reported here (most importantly, that in loaded joints) are far too experimentally critical and important to not be further tested and confirmed. Moreover, future extensions of the investigative protocols to the knee and ankle can supply a more complete picture of the dissipation of mechanical energy and therefore the necessity of a cost of transport which is more consistent in many forms of both natural and augmented locomotion.

References

Aleshinsky SY (1986a). An energy 'sources' and 'fractions' approach to the mechanical energy expenditure problem – I. Basic concepts, description of the model, analysis of a one-link system movement. J. Biomech. 19:287-293.

Aleshinsky SY (1986b). An energy 'sources' and 'fractions' approach to the mechanical energy expenditure problem – II. Movement of the multi-link chain model. J. Biomech. 19:295-300.

Aleshinsky SY (1986c). An energy 'sources' and 'fractions' approach to the mechanical energy expenditure problem – III. Mechanical energy expenditure reduction during one link motion. J. Biomech. 19:301-306.

Aleshinsky SY (1986d). An energy 'sources' and 'fractions' approach to the mechanical energy expenditure problem – IV. Criticism of the concept of 'energy transfers within and between links'. J. Biomech. 19:307-309.

Alexander RM (1989). Optimization and gaits in the locomotion of vertebrates. Phys. Rev., 69:1199-1227.

Barnett CH, Cobbold AF (1962). Lubrication within living joints. J. Bone and Joint Surg., 44B:662-674.

Blickhan R (1989) The spring-mass model for running and hopping. J. Biomech., 22:1217-1227.

Cavagna GA, Saibene FP, Margaria R (1963). External work in walking. J. Appl. Physiol., 18:1-9

Cavagna GA, Saibene F, Margaria R (1964). Mechanical work in running. J. Appl. Physiol. 19:249-252

Cavagna GA (1975). Force platforms as ergometers. J. Appl. Physiol., 39:174-179.

Cavagna GA, Thys H, Zamboni A (1976). The sources of external work in level walking and running. J. Physiol., 262:639-657.

Cavagna GA, Heglund NC, Taylor CR (1977a). Mechanical work in terrestrial locomotion: two basic mechanisms for minimizing energy expenditure. Am. J. Physiol., 233(5): R243-R261.

Cavagna GA, Kaneko M (1977b). Mechanical work and efficiency in level walking and running. J. Physiol., 268:467-481.

Cavagna GA, Franzetti M (1986). The determinants of the step frequency in walking in humans. J. Physiol., 373:235-242.

Charnley J (1960). The lubrication of animal joints in relation to surgical reconstruction by arthroplasty., Ann. Rheum. Dis., 19(1):10-19.

Crisco JJ, Blume J, Teeple E, Fleming BC, Jay GD (2006). Assuming exponential decay by incorporating viscous damping improves the prediction if friction in pendulum tests of whole articular joints., J. Eng. in Med., 221(H):325-333.

Francescato MP, Girardis M, di Prampero PE (1995). Oxygen cost of internal work during cycling. Eur. J. Appl. Physiol. 72:51-57.

Fukunaga T, Kubo K, Kawakami Y, Fukashiro S, Kanehisa H, Maganaris CN (2001). *In vivo* behavior of human muscle tendon during walking. Proc. R. Soc. Lond.,

268:229-233.

Fenn WO (1930). Frictional and kinetic factors in the work of sprint running., Am. J. Physiol., 92:583-611.

Jones ES (1934). Joint lubrication. The Lancet., 1:1426 – 1427.

Jones ES (1936). Joint lubrication. The Lancet., 230:1043-1044.

Margaria (1976). Biomechanics and energetics of muscular exercise. Clarendon Press, Oxford.

Maganaris CN, Paul JP, (2002). Tensile properties of the in vivo human gastrocnemius tendon. J. Biomech., 35:1639-1646.

Minetti AE, Saibene F (1992). Mechanical work rate minimization and freely chosen stride frequency of human walking: A mathematical model. J. Exp. Biol., 170:19-34.

Minetti AE (1998a). A model equation for the prediction of mechanical internal work of terrestrial locomotion. J. Biomech., 31:463-468.

Minetti AE (1998b). The biomechanics of skipping gaits: a third locomotion paradigm? Proc. R. Soc. Lond., 265:1227-1235.

Minetti AE (1999). The link between mechanics and energetics of locomotion. Proceedings of the XVIIth Congress of the International Society of Biomechanics. Calgary.

Minetti AE, Saibene F (2003). Biomechanical and physiological aspect of legged locomotion in humans. Eur J. Appl. Physiol., 88:297-316.

Minetti AE (2004). Passive tools for enhancing muscle-driven motion and locomotion. J. Exp. Biol., 207:1265-1272.

Minetti AE (2011). Bioenergetics and biomechanics of cycling: the role of 'internal work'. Eur. J. Appl. Physiol., 111:323-329.

Pavei G, Seminati E, Cazzola D, Minetti AE (2017). On the estimation accuracy of the 3D body center of mass trajectory during human locomotion: Inverse vs. Forward dynamics. Front. Physiol., 8:129.

Pavei G (2014). The effects of gravity on human locomotion repertoire: Cost of transport & body centre of mass analysis. Doctoral Thesis.

Peltonen J, Cronin NJ, Stenroth L, Finni T, Avela J (2013). Viscoelastic properties of the Achilles tendon in vivo. SpringerPlus., 2:212.

Stanton TE (1923). Boundary lubrication in engineering practice. *The Engineer*., 135:678-680

Steidel RF Jr. (1989). An introduction to mechanical vibrations, Wiley, New York.

Unsworth A, Dowson D, Wright V (1975a). The frictional behavior of human synovial joints – part I: Natural Joints. J. Lubrif. Tech., 97:369-376

Unsworth A, Dowson D, Wright V (1975b). Some new evidence on human joint lubrication. Ann. Rheum. Dis., 34:277-285.

van Ingen Schenau GJ, Cavanagh PR (1990). Power equations in endurance sports. J Biomech 23:865-881.

Willems PA, Cavagna GA, Heglund NC (1995). External, internal and total work in human locomotion. J. Exp. Biol., 198:379-393.

Williams KR, Cavanagh PR (1983). A model for the calculation of mechanical power during distance running. J. Biomech., 16:115-128.

Winter DA (1979). A new definition of mechanical work done in human movement. J. Appl. Physiol. 46(1):79-83.

Winter DA (2009). Biomechanics and motor control of human movement, Wiley, New York.

Woledge RC, Curtin NA, Homsher E (1985) Energetic Aspects of Muscle Contraction. Academic Press, London. (Monographs of the Physiological Society, vol. 41).